KINEMATIC ANALYSIS OF A THUMB-EXOSKELETON SYSTEM FOR POST STROKE REHABILITATION

By

Vikash Gupta

Thesis

Submitted to the Faculty of the

Graduate School of Vanderbilt University

in partial fulfillment of the requirements

for the degree of

MASTER OF SCIENCE

in

Mechanical Engineering

August, 2010

Nashville, Tennessee

Approved:

Professor Nilanjan Sarkar

Professor Derek Kamper

Professor Robert Webster III

ACKNOWLEDGEMENTS

I will like to extend my sincere thanks to Dr. Nilanjan Sarkar for his continuous support and guidance, for his encouragement and advice throughout my studies. He has always been a source of inspiration for me. I would also like to thank Dr. Derek Kamper from Rehabilitation Institute of Chicago, for providing valuable comments on the thesis and being supportive throughout the research.

My deep gratitude and sincere thanks goes to my parents and my sister, Swati Gupta. Their invaluable support, understanding and encouragement from far home has always helped me to continue my research. I would also like to thank Hari Kr. Voruganti, Mukul Singhee, Abhishek Chowdhury, Sayantan Chatterjee and Raktim Mitra for their support.

My sincere thanks goes to Nino Dzotsenidze, who has always supported and believed in me and helped me make the right decisions at all times. Without her support and encouragement, it would have not been possible.

I would also like to thank and express my sincere gratitude to my colleagues and friends Milind Shashtri, Furui Wang, Yu Tian, Jadav Das and Uttama Lahiri at Robotics and Autonomous Systems Laboratory for their support.

Last but not the least, I want to express my humble thanks and appreciation to Suzanne Weiss from the Mechanical Engineering department for always being supportive. I would also like to thank Liz Leis, from the Graduate School at Vanderbilt University for helping me in formatting the thesis and put it in the final shape.

LIST OF FIGURES

Figure Page

1. Five-link model of thumb 7
2. Thumb abduction to adduction (Right hand) 9
3. Thumb extension to flexion (Right hand) 10
4. Utah-MIT dexterous hand 12
5. Prototype of hand exoskeleton 14
6. Exoskeleton glove for paralyzed hands 15
7. Thumb and exoskeleton 18
8. Universal joint 19
9. Prototype of the exoskeleton 20
10. Thumb exoskeleton assembly with flexible shafts 21
11. Control flow diagram with open-loop control 34
12. Trajectory of the thumb-tip 35
13. Errors in constraints on metacarpal bone 36
14. Errors in constraints on proximal phalange 36
15. Errors in constraints on distal phalange 37
16 Variation of joint angles of thumb 38
17. Variation of active joint angles of exoskeleton 38
18. Variation of passive joint angles of exoskeleton 39
19. Control flow diagram for CLIK 42
20. Trajectory of the thumb-tip (CLIK) 43

21. Convergence of errors in X, Y and Z directions 44
22. Errors in constraints on Metacarpal segment 45
23. Errors in constraints on proximal phalange 45
24. Errors in constraints on distal phalange 46
25. Variation of joint angles of thumb 47
26. Variation of active joint angles of exoskeleton 47
27. Variation of passive joint angles of exoskeleton 48
28. Redundancy resolution 53
29. Trajectory of the thumb-tip in Cartesian space 54
30. Convergence of errors in the desired and actual trajectory 55
31. Errors in constraints on metacarpal segment 56
32. Errors in constraints on proximal phalange 56
33. Errors in constraints on distal phalange 57
34. Variation of joint angles of the thumb 58
35. Variation of active joint angles of exoskeleton 59
36. Variation of passive joint angles of exoskeleton 59
37. Comparison of joint angles of thumb (1of 2) 60
38. Comparison of joint angles of thumb (2 of 2) 61

TABLE OF CONTENTS

Page

ACKNOWLEDGEMENTS ii

LIST OF FIGURES iii

CHAPTER

I. INTRODUCTION 1

Problem Statement 3
Overview 3

II. LITERATURE SURVEY 4

Modeling the thumb 4
Description of thumb motion 9
Adduction-Abduction 9
Flexion-Extension 10
Range of motion of thumb 10
Existing rehabilitation devices 11

III. DESIGN OF EXOSKELETON 17

Mechanical design 17
Design of attachment 19
Transmission 21
Aligning the axes of thumb and the exoskeleton at CMC 21
DH-parameters for exoskeleton 22

IV. KINEMATIC ANALYSIS OF COUPLED EXOSKELETON-THUMB SYSTEM 24

Forward kinematics 24
Finding a feasible configuration 26
Inverse kinematics 29
Constraints 30
Open-loop Control 33

V. CLOSED-LOOP KINEMATIC ANALYSIS WITH REDUNDANCY RESOLUTION 40

Closed-loop inverse kinematics (CLIK) 40
Joint limit avoidance for the redundant manipulator 48
Redundancy resolution at velocity and acceleration levels..... 46
Result..... 53
Comparison of motion of thumb with
and without the application of joint limits 60

VI. CONTRIBUTIONS AND FUTURE WORK..... 62

Contributions 62
Future work 63

REFERENCES..... 64

CHAPTER I

INTRODUCTION

Stroke is defined as sudden, focal neurological deficit due to cerebrovascular abnormality. It is the third leading cause of death in the United States after heart disease and cancer. Each year, there are roughly 600,000 new stroke cases in the United States. About 1.1 million stroke survivors reported some degree of functional limitation in 1999 (American Heart Association, 2009). 30% of stroke survivors require assistance for walking and about 25% of the survivors require assistance for activities of daily living.

According to a recent survey by the National Stroke Association, 65% of the people in the United States who survived stroke are living with certain level of disability. These impairments among patients lead to loss of range of motion and diminished ability to generate force in the affected limbs. Impairment of the upper extremity is one of the major outcomes of a variety of neuromuscular disorders. Persistent deficits in motion, due to stroke are prevalent in distal upper extremities. Flexion-extension of the fingers is especially affected due to stroke (Trombly, 1989). Disability of distal hand function directly influences the patient's life by reducing effective self-care and employment opportunities.

A large amount of research has been done in order to improve the function of the upper extremity. Recent studies show that the brain can be remodeled after stroke. Task-specific and repetitive exercises are the key factors in promoting synaptogenesis and are central elements in rehabilitation of post-stroke motor weakness. Robotics, functional electrical

simulations, constraint-induced movement therapy (CIMT) and virtual reality are the major techniques used for post-stroke rehabilitation. In CIMT, the concept of forced use of the affected arm is emphasized, while the unimpaired arm is physically restrained with a sling. In addition, the therapist provides hand-over-hand skilled guidance to assist in repeated functional tasks. This kind of assisted training is very time-consuming for the therapist. Thus, robots are increasingly being developed and used to provide greater opportunity for rehabilitation. Robot assisted therapy has notable advantages over the conventional therapy, such as, increased intensity, more repetitions, better patient engagement and standardization of motion (O'Dell, Lin & Harrison, 2009).

Rehabilitation of the hand is important because the fingers and thumb play an important role in performing everyday tasks. Various robotic rehabilitation devices have been developed to assist in rehabilitation of the fingers and the thumb, which are discussed in the next chapter. The motion of the thumb is less understood and is more complicated than the fingers, while being the most important digit in the human hand. The present available devices address the issue of rehabilitating fingers, but none of them address the issue of independent control of the thumb joints, as it is discussed in the next chapter. The thumb provides us the ability to perform a variety of mundane tasks in our day-to-day life. The human thumb is opposable, which helps us to perform a huge variety of tasks. A thumb is called opposable, if it is able to manipulate in such a way so as to be able to touch all the four digits of the hand.

This thesis concentrates on rehabilitation of the thumb using an exoskeleton. When the patients loose their ability to move the thumb, one of the two possible cases might happen, either the joints of the thumb become stiff or they become fluid. In both the cases

one fails to perform the mundane tasks of daily life. Another important function of the thumb is to be able to generate the required thumb-tip forces for performing the tasks like pinch and grasp. So, both position and force control of the thumb is equally important for a person.

1.1 Problem Statement

The thesis addresses the following issues related to thumb rehabilitation:

1. Design an exoskeleton for thumb.
2. Design a general framework for mathematical modeling of the thumb and the designed exoskeleton.
3. Check for the validity of the exoskeleton design in order to validate the natural motion of the coupled thumb-exoskeleton system.

1.2 Overview

In this thesis, the exoskeleton design is discussed followed by a development of a general mathematical framework for modeling the thumb and the proposed exoskeleton. Subsequently, a kinematic analysis of the thumb-exoskeleton system is provided. The thumb-exoskeleton is a redundant manipulator, thus redundancy resolution for avoiding the natural joint limits of the thumb is applied during the motion of the thumb.

CHAPTER II

LITERATURE SURVEY

In this chapter, a literature survey of different types of thumb models as suggested by various researchers is discussed. This section also discusses the fundamental motions of the thumb and the techniques used in the past to understand the nature of thumb motion. Later on, it presents a brief description of the existing rehabilitation devices, their advantages and drawbacks.

2.1 Modeling the Thumb

The thumb's structure varies for each individual and that is one reason why researchers find it extremely difficult to model and parameterize the thumb. The human thumb consists of three bones namely metacarpal, proximal phalanx and distal phalanx starting from the base of the thumb to the tip. The metacarpal bone rests on the base called trapezium. The respective joints are carpometacarpal (CMC) joint, metacarpophalangeal (MCP) and the interphalangeal (IP) joints. Over the past few years, researchers suggest various types of thumb models. A three dimensional dynamic model of thumb having four degrees of freedom, with a universal joint at the CMC joint and revolute joints at the MCP joint and the IP joints is suggested (Esteki & Mansour, 1997). A representative model of each joint of the thumb is suggested on the basis of the architecture of the pertinent joint and its dominant motion (Cooney & Chao, 1977). The interphalengeal (IP) joint is represented by a hinge joint because it permits only flexion-extension motion. The

metacarpophalangeal (MCP) joint is roughly estimated as a universal joint. It is comprised of a biconvex surface on the metacarpal head and a slightly concave surface of the proximal phalanx. This ball-and-socket configuration allows relative free motion in all of the planes (Cooney & Chao, 1977). Thus, this joint has two DOF, adduction-abduction and flexion-extension. The thumb carpometacarpal (CMC) joint is composed of two-saddle shaped surfaces and the convexity of the metacarpal bones tightly fits the concave surface of the trapezium. This joint is also represented by a universal joint and has the same two DOFs as the MCP joint.

Though, the above description accounts for the motion of the thumb, the above kinematic model fails to account for the accurate thumb motion when all the joints move together. Anatomical studies and simulations suggest that the axes of rotation of the thumb are not perpendicular to each other. It has been conclusively proven that the CMC joint has two axes, one each in the trapezium and the metacarpal bones (Hollister, Buford & Myers, 1992). Similar studies show that the MCP joint has two offset axes, one in the metacarpal and one in the proximal phalanx, whereas, the interphalangeal joint axis is offset in two planes. They reported that motion about these axes result in congruent joint motion.

The kinematic model of the thumb was revised to account for these changes in the rotation of axes (Giurintano, Hollister, Buford, Thompson & Myers, 1995). The thumb was modeled as a virtual-five link manipulator with the links connected by hinge joints. This model also has same number of DOFs as the previous models. This model may seem counter-intuitive to the usual notion, as the thumb has only three bones, but the validity of the five-link thumb model is proven through experiments and it has been conclusively stated that the previous models do not represent the normal anatomy.

As stated earlier, the thumb parameters vary for each individual. Studies were conducted on the anatomic variability of the Denavit-Hartenberg parameters for the five-link model of thumb were reported (Santos & Valero-Cuevas, 2006). In this study, accounted for the anatomic variability of the thumb among different individuals. The virtual five-link description of the thumb depicts the thumb as a serial chain manipulator of five links. The 2-D anatomical projections were successfully transformed into Denavit-Hartenberg notations. They concluded the presence of four different types of kinematic models using Monte-Carlo simulations on 3550 D-H parameter sets of thumb. These simulations also helped in creating the representative models of each of the different types of thumb models. The above mentioned gives the kinematic structure of the thumb in terms of standard robotic convention (D-H parameters), which enables us to recreate the model of the thumb in the simulation environment of MatLab and SimMechanics. The authors categorized the DH parameter set into four types, referred to as Type I, Type II, Type III and Type IV. In our simulation, we have used the Type 2 kinematic model of the thumb provided by the above-mentioned authors.

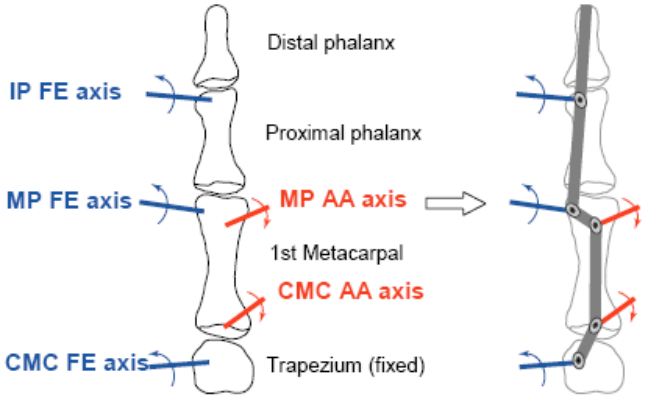

Figure 1 Five-link model of thumb (Santos & Valero-Cuevas, 2006)

In Figure 1, the kinematic model of thumb is shown (Santos & Valero-Cuevas, 2006). The flexion-extension and the adduction-abduction axes are described. The equivalent kinematic model of the thumb is also shown in the above figure. This configuration is considered the home position in our simulations.

The Denavit-Hartenberg parameters for the thumb are taken from a previous study (Santos & Valero-Cuevas, 2006). The authors successfully transformed the five DOF of the thumb from 2-D anatomical projections into the standard DH conventions. As mentioned earlier, they reported four types of kinematic models for the thumb, namely Type I, Type II, Type III and Type IV. They also report representative models of all the four types of kinematic models of the thumb. In our study, we chose the Type II representative model for further analysis. The DH parameters for the Type II model of the thumb as mentioned are as follows

Table 1 DH parameters of the Thumb (Type II), (Santos and Valero-Cuevas, 2006)

i	α_i	a_i	d_i	θ_i	**Motion**
z_1	-101.41	-3.8	8	0	Fixed
z_2	-75.03	14.7	-3.5	-104.22	CMC FE
z_3	70.77	32.2	16.1	23.07	CMC AA
z_4	111.73	0.5	1	200.7	MCP FE
z_5	106.14	43.5	-18.2	160.35	MCP AA
z_6	98.35	0	-11.1	70.2	IP FE
z_7	0	-1.8	36.4	0	Fixed

These DH parameters corresponding to z_1 take the transformations from the global co-ordinate system to the base of the CMC joint. The remaining transformations corresponding to z_2 through z_6 are the five axes of rotation. The last transformation z_7 corresponds to the thumb-tip reference axis. The global Cartesian coordinate system is centered at the proximal base of the trapezium and the axes are oriented as follows: +X = palmer, +Y = radial, +Z = distal.

2.2 Description of Thumb motion

The motion of thumb is complicated, because of the inherent complications in the kinematic structure as discussed in the previous sections. The function of the thumb in performing all the hand gestures is quite evident in the day-to-day life of human beings. The five-link kinematic structure of the thumb as depicted earlier captures the natural motion of the thumb more closely than previous models. Santos and Valero-Cuevas tried to approximate the structure of the thumb with hinged linkages and universal joints at the CMC and the MCP joints, but found that this approximate model fails to realistically predict the 3-dimensional static thumb-tip forces. The thumb motion can be categorically discussed under these types,

2.2.1 Adduction – Abduction

A motion, which pulls the limb (thumb) towards the mid-line of the body (index-finger) is called adduction. Similarly, the motion, which pulls the thumb away from the index finger, is called abduction.

Figure 2 Thumb abduction to adduction (right hand)

2.2.2 Flexion-Extension

A bending movement that decreases the angle between the two parts of the body is called flexion. Similarly, the opposite of this motion, that is, a movement, which increases the angle between the two parts of the body, is called extension. In the thumb, flexion-extension can be achieved by moving the thumb away from the fingers and across the palm.

Figure 3 Thumb extension to flexion (right hand)

Another important consideration in creating a realistic model of the thumb is that it should produce the required thumb-tip force for performing various tasks like pinch and grasp along with being able to display the full-range motion of thumb.

2.3 Range of motion of thumb

Range of motion of thumb refers to the total angle of rotation of each joint. Each joint of the thumb has a specific range of motion, which is expressed in degrees. For patients suffering from stroke, this normal range of motion is limited because of loss of motor

control or swelling or number of other causes. We intend to restore the normal range of motion of the thumb through rehabilitation and controlling the exoskeleton along with the thumb. Thus, it is important to have knowledge of the normal range of motion of the thumb.

Electrogoniometers were used on right-handed men to obtain the joint- measurements (Hume, Gellman, McKellop & Brumfield, 1990). The authors reported the functional range of MCP joint as 10-32˚, and that of IP joint as 2-43˚. In another study, roentgenographs were used (Cooney & Chao, 1977) and it was found that the interphalangeal (IP) joint has a range of 0-65˚ with little or no rotation during pinch and grasp. The MCP joint has a flexion-extension range of 10-40˚ and an adduction-abduction range of 0-15˚ during tip and palmer pinch.

2.4 Existing Rehabilitation Devices

Researchers (Riener, Nef and Colombo 2005) have shown that task-oriented repetitive movements can improve muscle strength and movement coordination among patients recovering from stroke. They show that rehabilitation robots can make the therapy of upper extremity functions more efficient, as the patients can be trained more intensively, while releasing the therapist from manual movement therapy. Moreover, the robotic rehabilitation systems can provide accurate quantitative measurements of the patient's performance.

Attempts to design an exoskeleton, which will restore motor control of the fingers and the thumb, have been made previously by many researchers. The task of designing an exoskeleton for thumb is challenging, as the motion of the thumb is inherently

complicated and there is limited understanding of the natural motion of thumb. Apart from that, the design should be adjustable in the sense that one should be able to attach the device on thumbs of various sizes. It should be compact and should be able to incorporate various sensors in it for joint angle measurement and also force sensing.

The MIT/Utah dexterous hand master (Figure 4) is one of the most known devices that is being used by researchers to understand the motion of the hand.

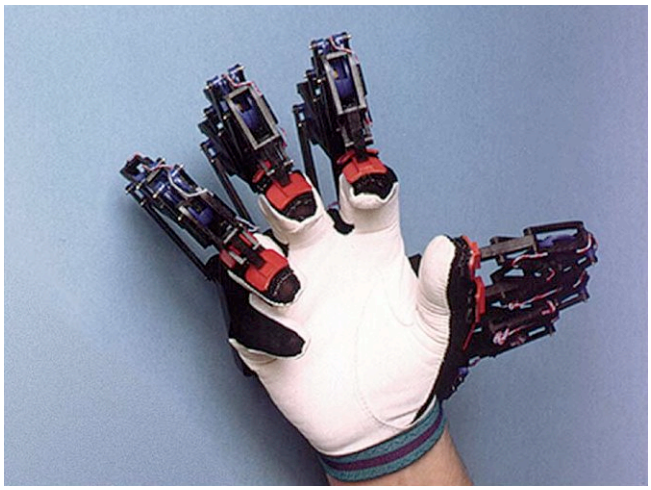

Figure 4 Utah-MIT Dexterous Hand (Sarcos Incorporated)

A similar product, which is commercially available, is called CyberGlove™. It can provide up to 22 precise joint angle measurements of the hand. The CyberGlove™ has been used in wide variety of real world applications like virtual prototype biomechanics and motion capture and animation. It is also one of the commonly used tools in understanding the thumb motion. Based on CyberGlove™ few virtual reality based experiments were designed for post stroke rehabilitation.

The PC-based virtual reality system was designed (Jack, Boian, Merians, Adamovich, Tremaine, Reece, Burdea and Poizner, 2000) using a CyberGlove™ and a RMII force feedback sensors for rehabilitation exercises. The CyberGlove™ is worn by the subject

and is used to measure the joint angles of thumb and the fingers during exercises, while the RMII glove is an exoskeleton device used to apply forces to the subject's finger tips and uses non-contact position sensors to measure the fingertip position with respect to the palm position. The forces are applied using lightweight pneumatic actuators attached to the tip of the thumb and the fingers. The subjects were involved in four different kinds of exercises each concentrating on range of motion, speed, independence of joint movements and strength of movements. These exercises take the form of target-based games and the user's performance is evaluated. The major concern in VR-based rehabilitation exercises is the transference of the skills-gained by the patient to the real world. Studies (Holden, 1999) show that though the VR-system is useful in learning motor skills, the knowledge is not always transferrable to real-world situations, while some others (Wilson, Forman and Stanton, 1997) disagree with the above notion.

VR Logic developed another device called CyberGrasp^{TM}, which is a haptic feedback device and is used for tele-manipulation. The device is a low-weight force-reflecting exoskeleton that fits over the CyberGlove^{TM} and add resistive feedback to each finger. The device allows full range motion of motion of the hand and is fully adjustable to fit a wide variety of hands. Researchers (Bergamasco, 1995) have used these devices for rehabilitating hand motion.

A double closed-loop control structure consisting of a position control loop and compensation control loop is developed (Shuang, Jiting, Yuru and Ju, 2009) for an exoskeleton with cable transmissions for index finger rehabilitation. This device had four degrees of freedom and consists of actuator and the exoskeleton modules. A DC motor with an encoder actuates the exoskeleton on the dorsal side of hand. To reduce the weight

on the patient's hand, the motors are kept far away from the hand and two cables in separate sheaths, the ends of which are connected on the actuator module and the exoskeleton module. These cables transmit the force and motion to the exoskeleton. A potentiometer is installed on the joint shaft of the exoskeleton, which measure the rotational angle of the PIP joint of the index finger. This exoskeleton design is controlled using a multi-layer control algorithm, and different algorithms for active and passive control modes are tested. The deflection of the sheath is modeled as a spring and the error caused by the deformation is compensated.

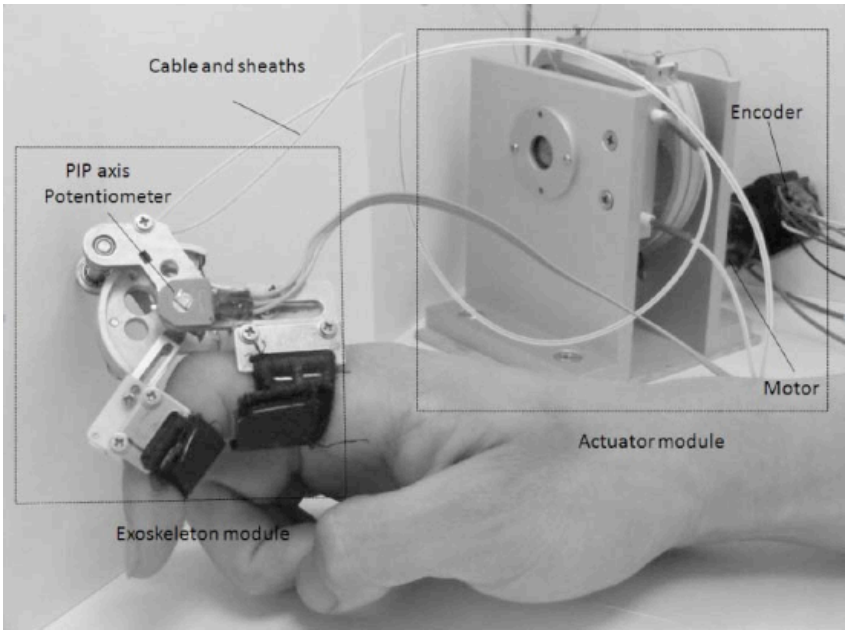

Figure 5 Prototype of the hand exoskeleton (Shuang, Jiting, Yuru and Ju, 2009)

An exoskeleton glove for controlling paralyzed hands (Brown, Jones and Singh, 1993) was designed, which considers only two primary motions of the thumb and fingers, flexion and extension. The exoskeleton was actuated using cables and springs, which were routed along the tendons on the thumb and finger. The tendons are responsible for

natural motion of thumb, so placement of cables along the tendons was important. The springs were placed in extended position along the thumb digits and the cables were used to retract the spring and achieve flexion. The design was limited and was not capable of executing intricate motions of the thumb. Also, the springs made the whole mechanism difficult to control and required large motor torque for control.

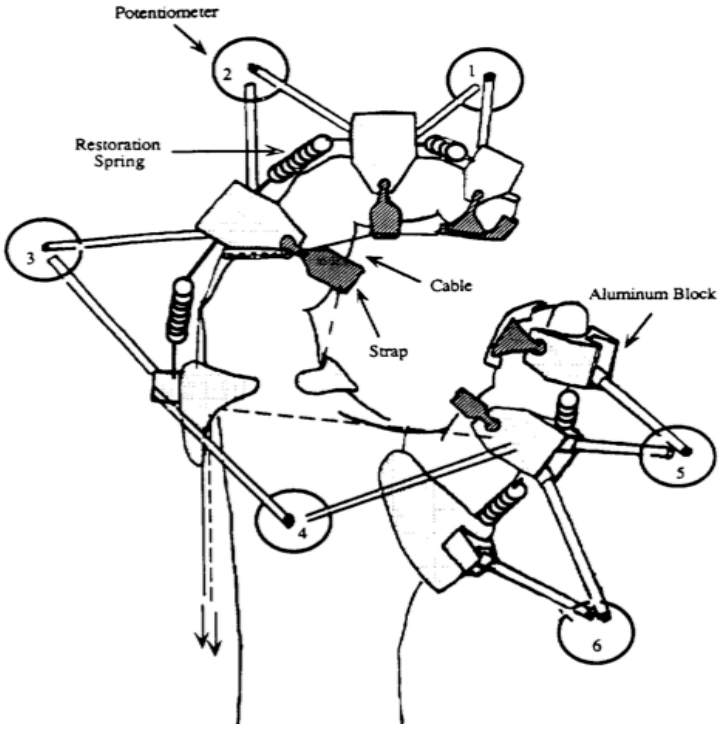

Figure 6 Exoskeleton glove for paralyzed hands (Brown, Jones and Singh, 1993)

While, the systems discussed above serve the purpose of hand rehabilitation, none of them specifically addresses the complicated thumb motions and allow independent control of all the joints of the thumb. In this thesis, the thumb is modeled as a five-degree of freedom serial manipulator, with virtual links connected by revolute joints. The exoskeleton design discussed in this thesis overcomes all the previously mentioned

issues, thus allowing independent control of the various joints of the thumb. The exoskeleton is actuated using flexible shafts, instead of the widely used cables and springs as in case of previous designs. The flexible shaft gives us the freedom of routing the transmission lines, which in case of cables are routed along the tendons.

CHAPTER III

DESIGN OF EXOSKELETON

The exoskeleton is designed to meet the following design requirements. From a mechanical point of view, it should be able to support motion of the thumb throughout the range of motion. It should also be lightweight and able to generate the required thumb-tip force for various hand gestures like pinch and grasp. In my work, I am trying to validate that the exoskeleton designed is able to generate the required thumb motion without any hindrance from the exoskeleton or the thumb or the other four fingers. Apart, from the motion constraints, it should also be lightweight so that the patient under rehabilitation does not feel uncomfortable or is tired easily because of the self-weight of the device. One major design aspect for the exoskeleton is the ability to control the different joints of the thumb independently. The thumb has five DOFs and so for each joint of the thumb, there is a corresponding joint on the exoskeleton, which maps its motion to the thumb.

Another important aspect of the design is that it should be adjustable and should encompass a wide range of thumbs for rehabilitation purposes. The exoskeleton was designed keeping all the above-mentioned criteria in mind.

3.1 Mechanical Design

The exoskeleton consists of 5 actuated joints and 3 passive joints, in order to achieve independent control of each joint. All the 8 joints of the exoskeleton are revolute.

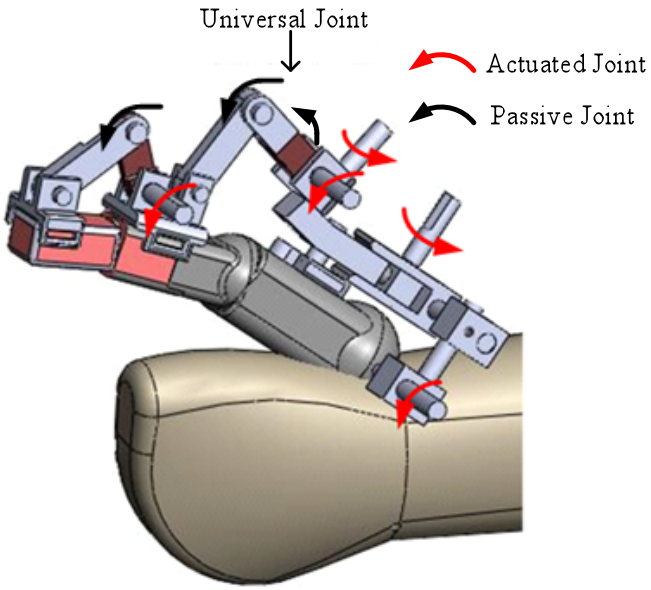

Figure 7 Thumb and Exoskeleton

The five actuated joints independently control the flexion/extension motion of the CMC, MCP and the IP joints and the adduction/abduction motion of the CMC and the MCP joint. As can be seen in Figure 7, the exoskeleton physically attaches to the distal, proximal, and metacarpal segments of the thumb. The base point for the motion of each segment is attached to the preceding segment. The attachment points are connected through two-bar linkages, which accommodate the variation in segment lengths across the population. Note that because the thumb joints are non-orthogonal and non-intersecting, a twisting motion will be observed between the CMC and the MCP joints when both joints move simultaneously. Thus a universal joint, which has 2 passive DOF, was developed for the thumb exoskeleton to allow this twisting motion, which is important for thumb opposition (Figure 8).

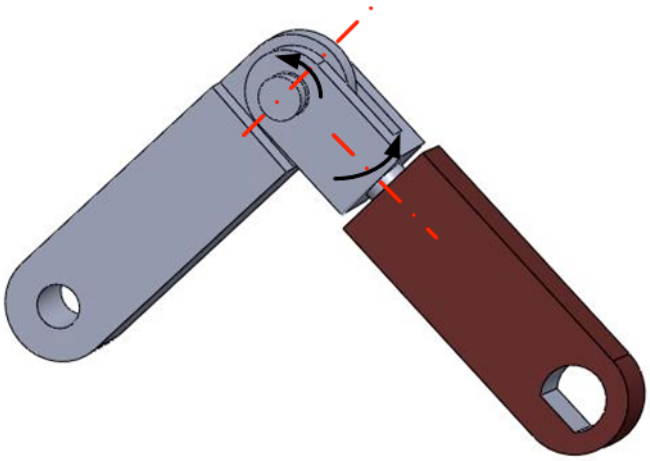

Figure 8 Universal joint

The five active joints are shown with red arrows in the Figure 7 and the two passive joints are in the universal joint and the third one is between the links connecting the proximal and the distal phalanx.

3.2 Design of Attachment

Designing the attachment module for coupling the exoskeleton and the thumb together is a challenging task. The major concern while designing the exoskeleton attachment is that it should not be so tight, that it causes discomfort to the user. On the other hand, it should not also be loose, otherwise effective motion and torque transmission from the exoskeleton to the thumb will not be possible, thus making the whole rehabilitation exercise futile. Apart from that, the attachment should also be in conformity with the thumb profile and should be adaptable enough to be used on a wide variety of population. An actual prototype of the exoskeleton is shown, with all the attachment modules in Figure 9.

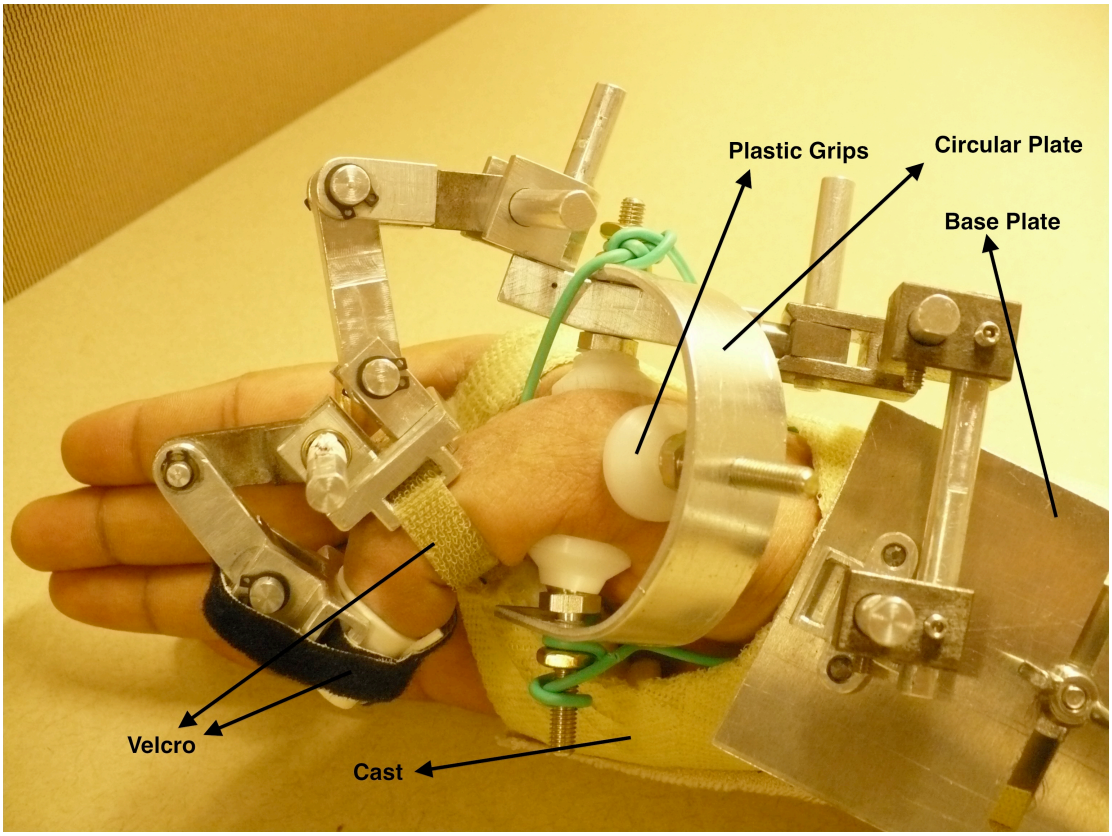

Figure 9 Prototype of the Exoskeleton

As can be seen in Figure 9, the attachment module is composed of a base plate, which is attached to a fiberglass cast worn over the arm. The base plate is bolted to the cast using screws. The proximal and the distal thumb segments are attached to the exoskeleton using Velcro. The metacarpal segment is attached to the exoskeleton using a semi-circular steel plate. Three screws pass through the steel plate, which can be tightened to attach the exoskeleton with the metacarpal segment. Flat ending plastic tips are attached to the screws; these plastic components interface with the patient's metacarpal segment. Also the underside of all exoskeleton attachment points is padded with foam to ensure firm and comfortable grip of the exoskeleton on the thumb.

3.3 Transmission

To minimize the load of the exoskeleton on the patient's hand, the actuators for the joints are located at a distance from the thumb-exoskeleton, and are supported on a tabletop. For torque transmission, flexible shafts from S.S. White are used. These flexible shafts can transmit rotary motion as well as torque from the motors to the shafts, while allowing off-axis movements of the exoskeleton with respect to the motors. As the torque requirement on the different joint of the thumb are different, flexible shafts of different diameters are chosen correspondingly. The smaller shafts can transmit less torque, but are lighter and have less inertia.

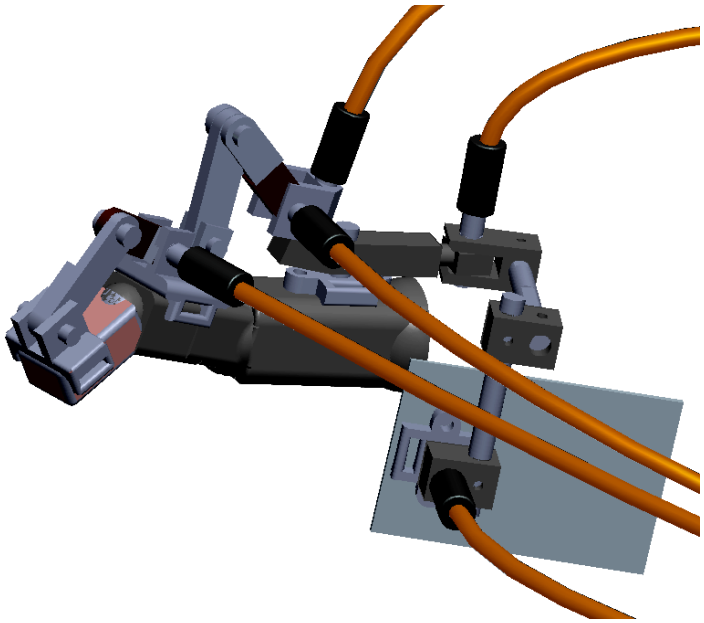

Figure 10 Thumb-exoskeleton assembly with flexible shafts

3.4 Aligning the axes of thumb and the exoskelet22on at CMC

The flexion-extension axis and the adduction-abduction axes at the CMC joint of the thumb are aligned with that of the exoskeleton. When the axes of the thumb and the

exoskeleton are aligned, the motion of the thumb-exoskeleton system is equivalent to that of two parallel links having the same axis of rotation. The benefit of such a design is that it reduces the number of constraint equations of constraints by one. For example, if two links are moving on a plane with their axes of rotation aligned with each other, and if we want to write the constraint equation for the end-tip, instead of writing the position equations for both the links for both $\boldsymbol{x}$ and $\boldsymbol{y}$ directions, one can just solve the equations to satisfy either of the coordinate and the other one is satisfied automatically. Thus, for a 2-D system the constraint equations reduce by one. Similarly, when considered for a 3D system, only two constraint equations ($\boldsymbol{x}$ and $\boldsymbol{y}$) need to be considered and the constraint in $\boldsymbol{z}$ direction is automatically satisfied. This reduction of constraint only works for the first point of contact on the metacarpal bone. For the remaining two points of attachment the equations of constraint on all the three directions needed to be solved. Thus, we end up with eight equations, which need to be solved for eight unknowns. This will yield a unique feasible configuration, which satisfies all the constraints.

3.5 DH parameters for exoskeleton

For all the calculations, and further modeling of the exoskeleton, the DH parameters of the exoskeleton were measured from the SolidWorks™ model of the exoskeleton. The parameters are listed in the Table 2. In order to align the axes of the exoskeleton and the thumb, the DH-parameters for the first three links of the exoskeleton were same as that of the Type II thumb (Santos & Valero-Cuevas, 2006).

Table 2 DH Parameters for exoskeleton

i	α_i	a_i	d_i	θ_i	*Nature of joints*
1	-101.41	-3.8	8	0	fixed
2	-75.03	14.7	-3.5	θ_1	active
3	70.77	32.2	16.1	θ_2	active
4	-90	10.16	0	θ_3	active
5	-90	0	0	θ_4	active
6	0	0	10	0	fixed
7	90	0	10	θ_5	passive
8	0	30	0	θ_6	passive
9	0	35	0	θ_7	active
10	0	35	0	θ_8	passive

CHAPTER IV

KINEMATIC ANALYSIS OF COUPLED EXOSKELETON-THUMB SYSTEM

This chapter discusses the coupled motion of the thumb-exoskeleton system. The chapter broadly describes the forward and inverse kinematics routines followed by an open-loop control scheme for the thumb-exoskeleton system. In the open-loop control scheme, the thumb-tip is made to follow a desired trajectory, without violating the constraints (points of attachment of the thumb and the exoskeleton) in the system. The constraints and their mathematical formulation are also described in this chapter.

4.1 Forward Kinematics

Forward kinematics is the study of the end effectors' position and orientation as a function of the joint angles of the manipulator. To each link of the manipulator co-ordinate frames are assigned and relationships between these frames are expressed using homogenous transformation matrices. A robotic manipulator is a set of links connected by joints. In our study, all the joints within the thumb and the exoskeleton are revolute. In robotics literature, the link parameters are defined by a set of Denavit Hartenberg (DH) parameters. In our study we have used the standard DH conventions for our analysis of the thumb and exoskeleton. The DH-parameters for the thumb are taken from a previous study (Santos & Valero-Cuevas, 2006). The authors successfully transformed the five DOFs of the thumb from 2-D anatomical projections into the standard DH conventions. As mentioned earlier, they reported four types of kinematic models for the thumb,

namely Type I, Type II, Type III and Type IV. They also report representative models of all the four types of kinematic models of the thumb. In our study, we chose the Type II representative model for further analysis. The DH parameters for the Type II model of the thumb are shown in Table 1.

They (Santos & Valero-Cuevas, 2006) also report the bounding-box bone dimensions, which are tabulated below,

Table 3 Bounding-box bone dimensions

Bone	Palmer (x) (mm)	Radial (y) (mm)	Distal (z) (mm)
Distal Phalanx	14.5	20.7	33.0
Proximal Phalanx	15	21.1	41.5
1st Metacarpal	17.3	16.8	49.8
Trapezium	14.0	21.9	15.9

For the standard DH conventions, the transformation matrix between two adjacent frames {i} and {i-1} is given by

$$ {}^{i}_{i-1}T = \begin{bmatrix} Cos\theta_i & -Sin\theta_i Cos\alpha_i & Sin\theta_i Sin\alpha_i & a_i Cos\theta_i \\ Sin\theta_i & Cos\theta_i Cos\alpha_i & -Cos\theta_i Sin\alpha_i & a_i Sin\theta_i \\ 0 & Sin\alpha_i & Cos\alpha_i & d_i \\ 0 & 0 & 0 & 1 \end{bmatrix} $$

, where ζ_i, a_i, d_i and θ_i refer to the parameters corresponding to the i^{th} joint. The exoskeleton is hinged to the thumb at three locations, one on each of the three bones

CMC, MCP and IP. Using the transformation matrices, the locations of the three points, where the exoskeleton and the thumb are hinged, can be found out.

For simulation purposes, **SimMechanics** models of the thumb and the exoskeleton are created using the DH-parameters of the thumb and the exoskeleton (Table 1 and 2). Two simulations run separately, one on SimMechanics and the other on matlab's symbolic toolbox. The SimMechanics toolbox offers a platform to make the physical models and also provides a visualization environment for the model. The transformation matrices are multiplied in the Matlab's symbolic toolbox environment, which gives the mathematical expression for the position in terms of the joint angles of the thumb. The results from both of the simulations were found to match, thus validating the models.

As mentioned earlier, the thumb and the exoskeleton are attached at three locations. The coordinates for each of these locations can be found using the transformation matrices described earlier.

4.2 Finding a feasible configuration

A feasible configuration for the thumb-exoskeleton system is one which satisfies all the required position constraints at the points of contact of the thumb and the exoskeleton. For reasons mentioned in the previous chapter, there are eight equations and eight unknowns for which we need to solve.

If $\boldsymbol{X_1}$, $\boldsymbol{X_2}$ and $\boldsymbol{X_3}$ are the three points where the exoskeleton and the thumb and exoskeleton are attached to each other, we can write the equations for the coordinates of all the three points using forward kinematics. The exoskeleton and the thumb are treated as two separate serial manipulators. Using the transformation matrices, the position

vectors for X_1, X_2 and X_3 are written in terms of the joint angles of the thumb. Similarly sets of equations are written in terms of joint angles of the exoskeleton.

Since, both set of equations refer to the same point, we can equate the corresponding equations. To find the eight joint angles of the exoskeleton for a given set of configurations for the thumb, we need to solve the eight equations numerically. We use the *fsolve* routine of MatLab to solve the equations. The criterion for an acceptable solution is that the solution set should be within the feasible range of motion of the thumb. The equations are cyclic in nature, so more often the solutions yield angles, which are not physically feasible (flipped cases). But, from the physical model of the exoskeleton, a fairly good estimate of the range of motion of joint angles of the exoskeleton can be found. A valid solution should also be the set of angles of exoskeleton, which are within the estimated joint-range.

The above problem of finding a feasible set of joint angles of the exoskeleton can be formulated as a constrained optimization problem. Let us define the function F and G as follows.

$$X_1 = F_1(\theta_1, \theta_2) \tag{1}$$

$$X_2 = F_2(\theta_1, \theta_2, \theta_3, \theta_4, \theta_5, \theta_6) \tag{2}$$

$$X_3 = F_3(\theta_1, \theta_2, \theta_3, \theta_4, \theta_5, \theta_6, \theta_7, \theta_8) \tag{3}$$

, where θ_i's are the joint angles of the exoskeleton and F_i's are the functions, which express the coordinates of X_1, X_2, and X_3. Also, the same points can also be expressed as a function of the joint angles of the thumb as mentioned earlier. Let G_i's be the function analogous to F_i's in terms of joint angles of thumb. So, we can write

$$X_1 = G_1(\xi_1, \xi_2) \tag{4}$$
$$X_2 = G_2(\xi_1, \xi_2, \xi_3, \xi_4) \tag{5}$$
$$X_3 = G_3(\xi_1, \xi_2, \xi_3, \xi_4, \xi_5) \tag{6}$$

, where ***ζ's*** are the joint angles of the thumb. It should be noted that $\boldsymbol{X_1}$ is a 2×1 vector, whereas, $\boldsymbol{X_2}$ and $\boldsymbol{X_3}$ are 3×1 vectors for reasons mentioned in previous chapter. So, ideally when all the constraints are satisfied we have ***F=G.***

If we define a vector ***H=F-G,*** and also define Δ as,

$$\Delta = \sum_{i=1}^{8} H(i)^2 \tag{7}$$

Our problem of finding the adequate values of joint angles becomes a constrained minimization problem, with Δ as the objective function. The constraints on the joint angles are as follows,

$$\left.\begin{aligned} -10^0 \le \theta_1 \le 10^0 \\ -10^0 \le \theta_2 \le 10^0 \\ -70^0 \le \theta_3 \le 10^0 \\ -200^0 \le \theta_4 \le -100^0 \\ -10^0 \le \theta_5 \le 70^0 \\ -60^0 \le \theta_6 \le 270^0 \\ -200^0 \le \theta_7 \le 0^0 \\ 0^0 \le \theta_8 \le 180^0 \end{aligned}\right\} \tag{8}$$

For solving the above problem, first an initial configuration is chosen for which the joint angles of the thumb are known and then the equations are solved to get the corresponding joint angles of the exoskeleton. This operation is carried out using the *fmincon* routine of MatLab. The initial conditions for the numerical simulations are chosen as joint angles halfway through the joint ranges. Though, this minimization yields fairly good results.

Another MatLab routine *fsolve* is used to solve the above equations numerically, with the results of the previous simulation as the initial guess for the *fsolve* routine.

The above operations yield the required joint angles for the exoskeleton, which are within the feasible joint range of motion of the exoskeleton. If the results are not satisfactory, both the operations are repeated again, until the solutions converge. In most of the simulations a good initial approximation makes convergence possible in approximately eight iterations.

4.3 Inverse Kinematics

Inverse kinematics is the study pertaining to finding the corresponding joint angles when the end-effectors' position is known. Thus if, forward kinematics gives us the expression of the form,

$$X = f(\theta) \tag{9}$$

Inverse kinematics as the name suggests refers to the following problem,

$$\theta = f^{-1}(X) \tag{10}$$

Most of the times, it is not likely, that a closed form solution for the joint angles in terms of the end-effectors' position can be found. Even if a closed form solution can be found, often there are multiple configurations (corresponding to the multiple solutions of the equations) of the manipulator, which yield the same end point. Other reason, for this kind of solution set is that the equations (9) are cyclic in nature.

In our problem, the equations being highly nonlinear, it is impossible to find a closed form solution for the joint angles of the exoskeleton or the thumb. Differentiating the position level equations linearizes the system. Thus, if $\boldsymbol{X_1}$, $\boldsymbol{X_2}$ and $\boldsymbol{X_3}$ are the three points

where the exoskeleton and the thumb are constrained, X_3 being the thumb-tip, X_1 and X_2 being the point of contact on the metacarpal bone and proximal phalange of the thumb respectively. We can write the following equations:

$$X_1 = F_1(\theta_1, \theta_2) \tag{11}$$

$$X_2 = F_2(\theta_1, \theta_2, \theta_3, \theta_4, \theta_5, \theta_6) \tag{12}$$

$$X_3 = F_3(\theta_1, \theta_2, \theta_3, \theta_4, \theta_5, \theta_6, \theta_7, \theta_8) \tag{13}$$

Differentiating (13) we have,

$$\dot{X}_3 = J_1 \dot{\theta} \tag{14}$$

$$\dot{X}_3 = [J_{1a} \quad J_{1p}] \begin{bmatrix} \dot{\theta}_a \\ \dot{\theta}_p \end{bmatrix} \tag{15}$$

$$\dot{X}_3 = [J_{1a} \dot{\theta}_a + J_{1p} \dot{\theta}_p] \tag{16}$$

, where J_1 is the 3×8 Jacobian matrix given by $J_1 = \frac{\partial F_3}{\partial \theta}$ and $\theta = [\theta_a \quad \theta_p]^T$ is the vector of eight joint angles of the exoskeleton. Also, θ_a ($\theta_1, \theta_2, \theta_3, \theta_4, \theta_7$) and θ_p ($\theta_5, \theta_6, \theta_8$) are the active and the passive joint angle vectors of the exoskeleton. J_{1a} and J_{1p} are the sub-matrices corresponding to the active and passive joint angles of the exoskeleton.

4.4 Constraints

In the exoskeleton – thumb mechanism there are eight holonomic constraints, which can be summarized as follows:

$$\overline{X}_1 : \overline{F}_1(\theta_1, \theta_2) = \overline{G}_1(\zeta_1, \zeta_2) \tag{17}$$

$$\overline{X}_2 : \overline{F}_2(\theta_1, \theta_2, ..., \theta_6) = \overline{G}_2(\zeta_1, \zeta_2, ..., \zeta_4) \tag{18}$$

$$\overline{X}_3 : \overline{F}_3(\theta_1, \theta_2, ..., \theta_8) = \overline{G}_3(\zeta_1, \zeta_2, ..., \zeta_5) \tag{19}$$

Since, the expressions $\boldsymbol{F_i}$ and $\boldsymbol{G_i}$ (i=1,2,3) represent the same point, equations 18, 19 and 20 represent the constraint equations for our system.

The above eight constraints (two constraints in the *x* and *y* direction for $\boldsymbol{X_1}$ and three on each of the Cartesian directions for $\boldsymbol{X_2}$ and $\boldsymbol{X_3}$) can be written in concise form as

$$\overline{H}(\theta_a, \theta_p, \zeta) = 0 \tag{20}$$

, where $\overline{H} = \overline{F} - \overline{G}$ and each of *H, F* and *G* are 8×1 vectors.

The system of equations (13) being highly nonlinear differentiation linearizes the system. So, differentiating (13) with respect to time, we have the following equations.

$$\frac{\partial \overline{H}}{\partial \theta_a}\dot{\theta}_a + \frac{\partial \overline{H}}{\partial \theta_p}\dot{\theta}_p + \frac{\partial \overline{H}}{\partial \zeta}\dot{\zeta} = 0 \tag{21}$$

$$\frac{\partial \overline{H}}{\partial \theta_p}\dot{\theta}_p + \frac{\partial \overline{H}}{\partial \zeta}\dot{\zeta} = -\frac{\partial \overline{H}}{\partial \theta_a}\dot{\theta}_a \tag{22}$$

$$\therefore \left[\left.\frac{\partial \overline{H}}{\partial \theta_p}\right|_{8\times 5} \quad \left.\frac{\partial \overline{H}}{\partial \zeta}\right|_{8\times 3}\right]\begin{bmatrix}\dot{\theta}_p \\ \dot{\zeta}\end{bmatrix} = -\left.\frac{\partial \overline{H}}{\partial \theta_a}\right|_{8\times 5}\dot{\theta}_a \tag{23}$$

Let us, represent the above Jacobians as follows,

$$\begin{bmatrix}\frac{\partial \overline{H}}{\partial \theta_p} & \frac{\partial \overline{H}}{\partial \zeta}\end{bmatrix} = J_{2_d} \tag{24}$$

, where $J_{2_d} \in \Re^{8\times 8}$ and

$$\frac{\partial \overline{H}}{\partial \theta_a} = J_{2_{\theta_a}} \tag{25}$$

Thus, substituting (24) and (25) in equation (23), we have

$$J_{2_d}\begin{bmatrix}\dot{\theta}_p \\ \dot{\xi}\end{bmatrix} = -J_{2_{\theta a}}\dot{\theta}_a \tag{26}$$

$$\therefore \begin{bmatrix}\dot{\theta}_p \\ \dot{\xi}\end{bmatrix} = -\left(J_{2_d}\right)^{-1} J_{2_{\theta a}}\dot{\theta}_a \tag{27}$$

$$\begin{bmatrix}\dot{\theta}_p \\ \dot{\xi}\end{bmatrix} = J_3\dot{\theta}_a \tag{28}$$

, where $J_3 = -\left(J_{2_d}\right)^{-1} J_{2_{\theta_a}}$.

Thus, simplifying further we get,

$$\begin{bmatrix}\dot{\theta}_p \\ \dot{\xi}\end{bmatrix} = \begin{bmatrix}J_{3_{\theta p}} \\ J_{3a}\end{bmatrix}\dot{\theta}_a \tag{29}$$

$$\therefore \dot{\theta}_p = J_{3_{\theta p}}\dot{\theta}_a \tag{30}$$

$$\dot{\xi} = J_{3_{\theta a}}\,\dot{\theta}_a \tag{31}$$

, where $J_{3_{\theta p}}$ and J_{3_a} are the sub-matrices of the matrix J_3. Clearly, $J_{3_{\theta p}}$ is a 3×5 matrix and J_{3_a} is a 5×5 matrix. Thus, equation (30) provides a relationship between the passive and active joint velocities of the exoskeleton, and similarly equation (31) provides a relationship between the thumb joint angle velocities and the active joint velocities of the exoskeleton. Again, substituting equation (30) in (16),

$$\dot{X}_3 = [J_{1a} + J_{1p}J_{3_{\theta p}}]\dot{\theta}_a \tag{32}$$

Let,

$$J = [J_{1a} + J_{1p}J_{3_{\theta p}}]$$

Thus, from equation (26), we have

$$\dot{X}_3 = J\,\dot{\theta}_a \tag{33}$$

$$\therefore \dot{\theta}_a = J^{\dagger}\,\dot{X}_3 \tag{34}$$

, where $J^{\dagger}$ is the pseudoinverse of J.The above equation gives us the required relation between the end-effector's velocity in task-space and the active joint angle velocities of the exoskeleton.

4.5 Open-loop Control

Two different configurations of thumb are chosen and using the forward kinematics the corresponding Cartesian coordinates of the thumb-tip are found. Let, $\boldsymbol{X_i}$ and $\boldsymbol{X_f}$ be the two above-mentioned points in the task-space corresponding to the two different configurations of the thumb. A minimum-jerk trajectory is fitted between these two points using a fifth-order polynomial. Differentiating the trajectory equation gives the desired velocity of the thumb-tip in the Cartesian space. The corresponding angular velocity of the active joint angles of the exoskeleton can be found using equation 34. The Jacobian $\boldsymbol{J}$ is a 3×5 matrix. So, the weighted pseudoinverse is calculated. Also, once the active joint angle velocities are known, the angular joint velocities of the passive joints and the corresponding joint velocities for the thumb can be computed too using equations 30 and 31. Finally the derivatives are integrated, with proper initial conditions corresponding to the initial point of the trajectory $\boldsymbol{X_i}$. The calculated angles are used to find the Cartesian coordinates of the end-effector of the exoskeleton, and the thumb-tip. It is expected that the thumb-tip will follow the desired trajectory, without violating the position constraints. It was found that throughout the trajectory, the errors between the thumb-tip and the exoskeleton were of the order of 10^{-5} mm.

The control flow diagram for the above control system is shown in Figure 11.

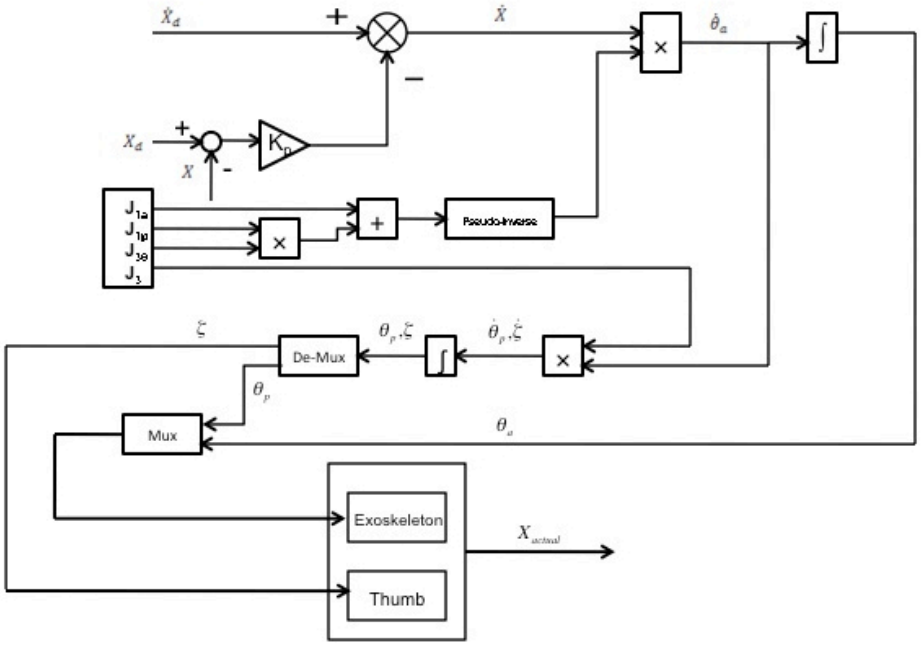

Figure 11 Control Flow Diagram for Open-loop Control

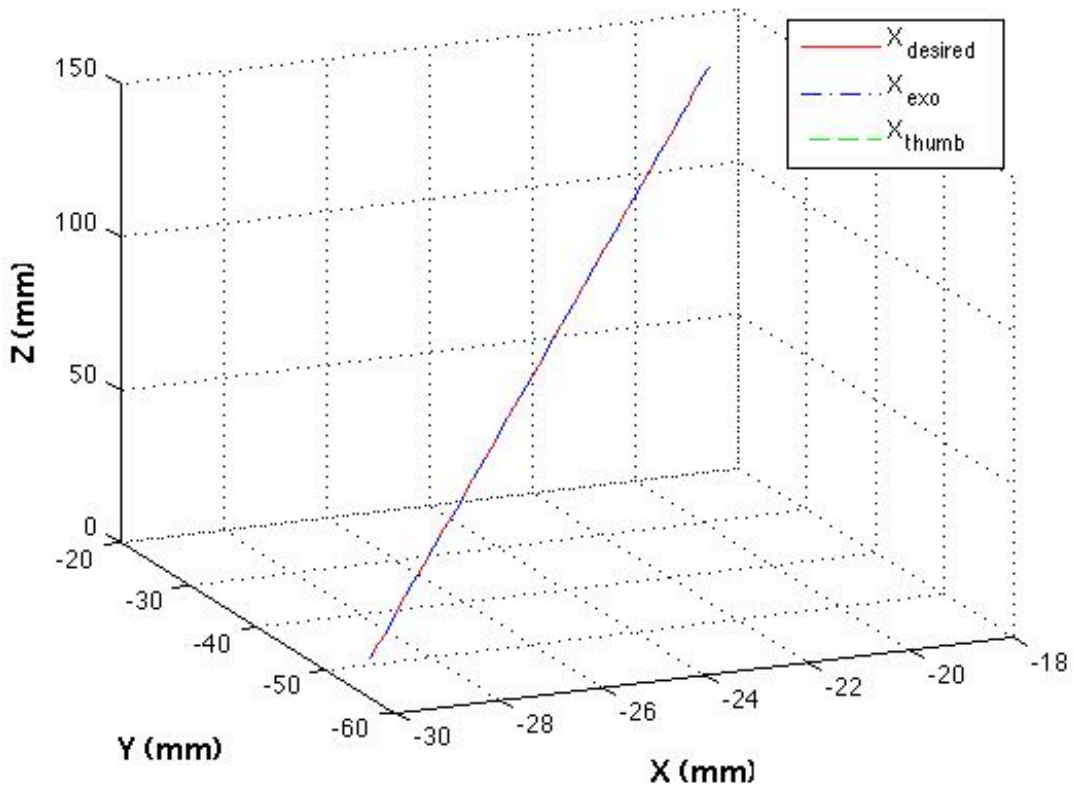

Figure 12 Trajectory of the thumb tip

The Figure 12 shows the minimum jerk trajectory followed by the thumb-tip in the Cartesian space between the points X_i=[-19.3299; -25.6866; 141.5799] and X_f=[-29.9388; -55.9788; 12.2515]. It can be seen that the both the thumb-tip and the exoskeleton follow the desired trajectory precisely.

Throughout the trajectory, all the three constraints are satisfied, which can be shown in the Figures 13-15.

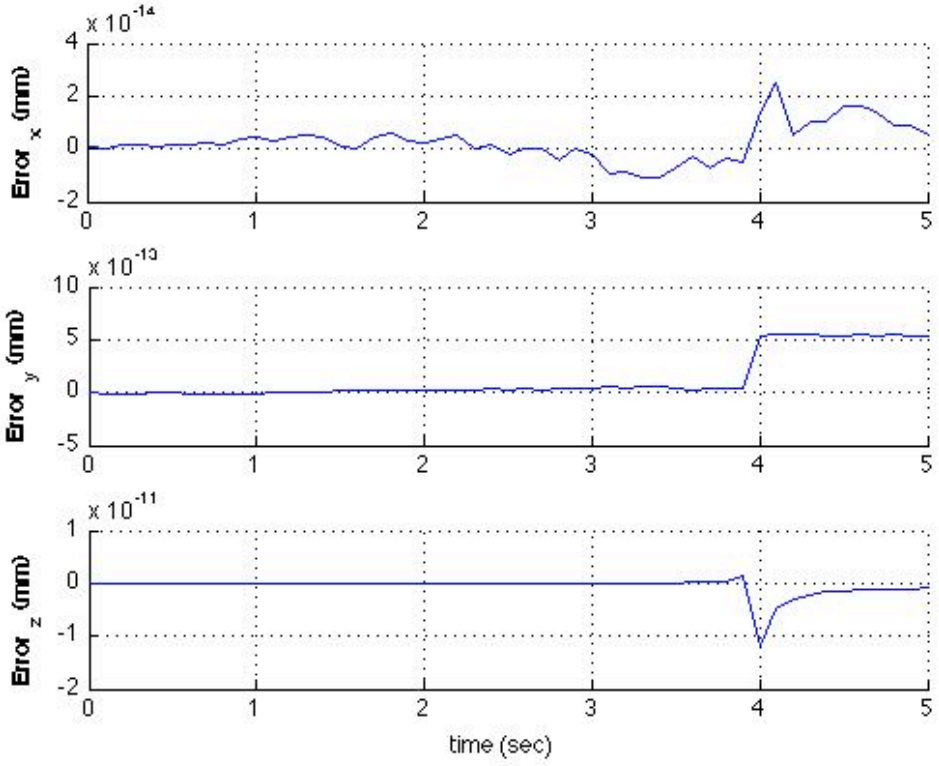

Figure 13 Errors in constraint on metacarpal bone (in mm)

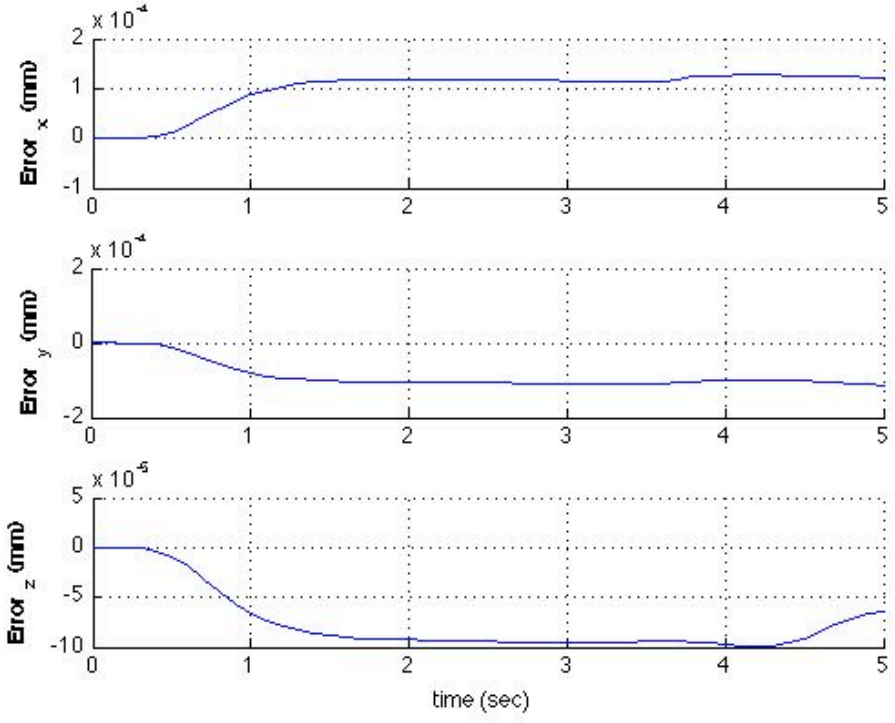

Figure 14 Errors in constraints on proximal phalange (in mm)

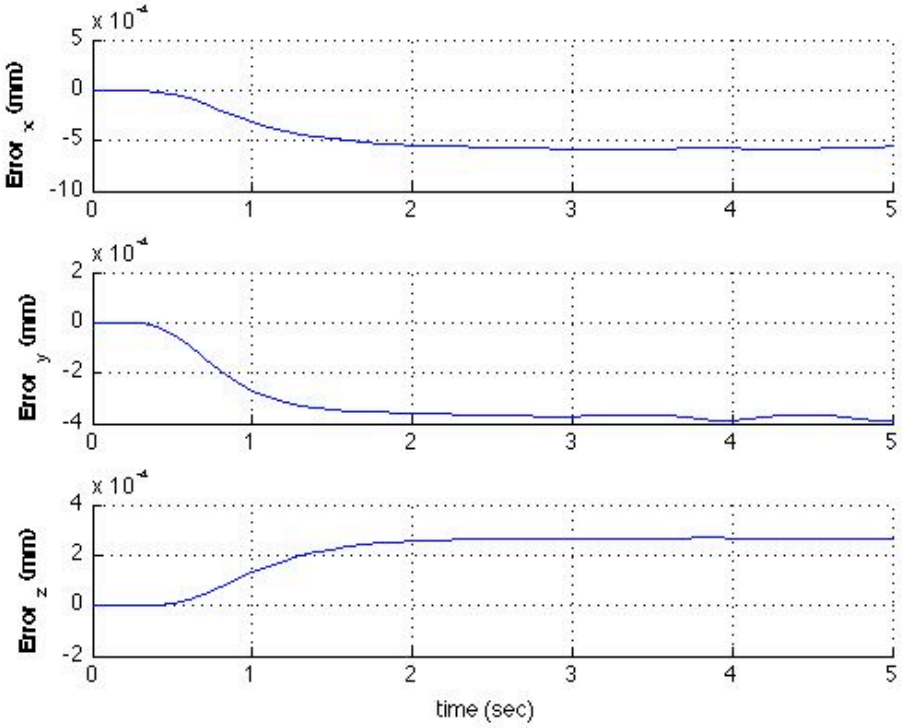

Figure 15 Constraint on distal phalange

The above figures (13-15) show the position errors between exoskeleton and the thumb at X_1, X_2 and X_3. It should be noted that the errors are of the order of 10^{-6} mm, throughout the trajectory, which is acceptable for all practical application.

The plots below show the variation of the joint angles of the thumb, active angles of the exoskeleton and the passive angles of the exoskeleton. As mentioned earlier, the position X_i (initial position) refers to a straight thumb configuration as shown in figure 5. So all the initial joint angles of the thumb are zero. The final angles at the end of trajectory correspond to the point X_f (final position) in the task-space.

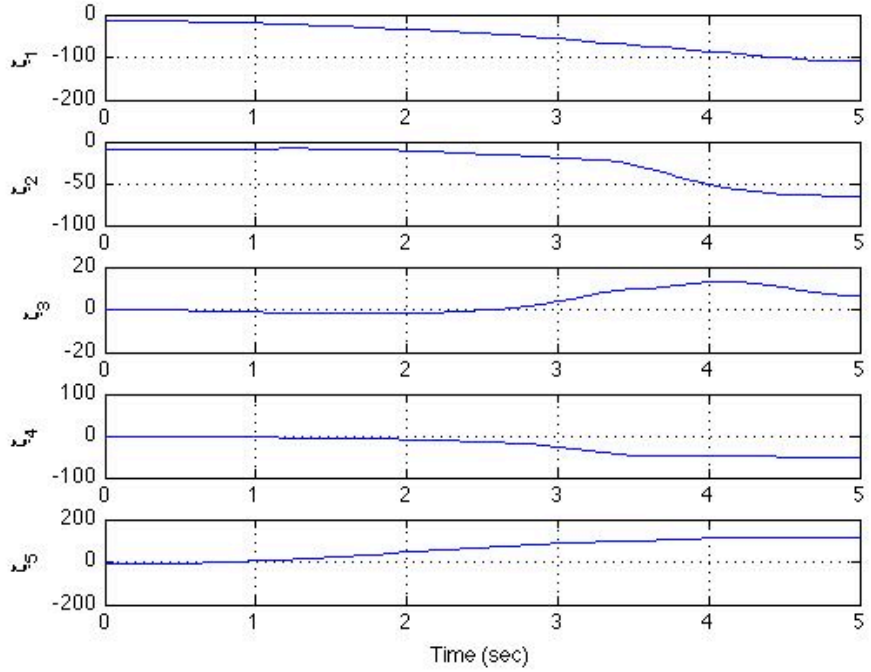

Figure 16 Variation of joint angles of thumb (in deg)

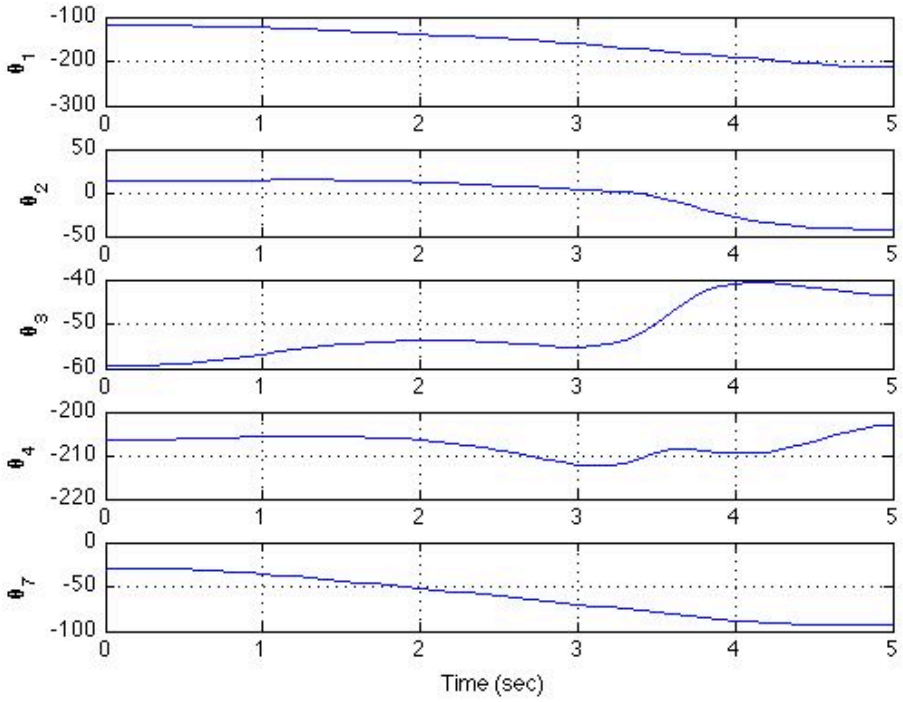

Figure 17 Variation in the active joint angles of exoskeleton

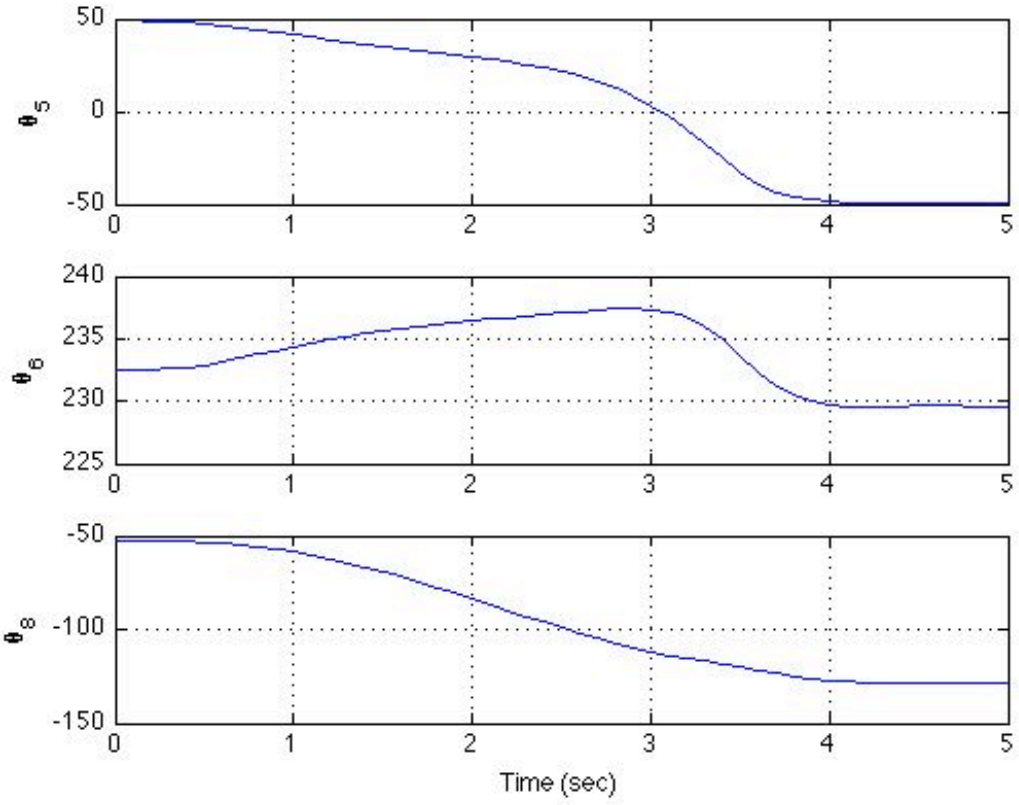

Figure 18 Variation in the passive joint angles of the exoskeleton

The figures 16-18 show that the variation of angles, which confirms with the joint range of motion discussed before. The above simulation was carried out for 100 second using *"ode45"* adaptive solver, the maximum and minimum step-size set to *auto* and the relative tolerance to 10^{-3}.

The above plots validate the exoskeleton design in the sense that the exoskeleton designed allows natural motion of the thumb without any hindrance.

CHAPTER V

CLOSED-LOOP KINEMATIC ANALYSIS WITH REDUNDANCY RESOLUTION

In the previous chapter the coupled motion of the thumb-exoskeleton system is discussed in detail. Along with the forward and inverse kinematics analysis, an open-loop control scheme was also discussed. In this chapter, we discuss a closed-loop inverse kinematics scheme for the coupled motion of the thumb-exoskeleton system. Later on, we also resolve the redundancy and exploit the redundancy to constraint the motion of the thumb within the natural limits of the motion.

5.1 Closed-Loop Inverse Kinematics (CLIK)

Chiacchio suggested closed-loop inverse kinematics (Chiacchio, Chiaverini, Sciavicco & Siciliano, 1991) scheme for constrained redundant manipulators. The thumb-exoskeleton has two degrees of redundancy, as the thumb has five degrees of freedom but the task-space is only three-dimensional. The CLIK scheme was also used for obstacle avoidance and joint-limit avoidance constraints (Sciavicco & Siciliano, 1987). For thumb, we do not need to consider the obstacle avoidance, as that is not a concern in the problem defined. Also, the joint limit criterion is taken into account while finding the initial conditions.

As, mentioned in the previous chapter, a minimum jerk trajectory is designed between the initial and the final point, $\boldsymbol{X_i}$ and $\boldsymbol{X_f}$ respectively. This is the desired trajectory that the thumb-tip should follow. Differentiating it twice, gives the desired acceleration of the

thumb-tip in the task-space. Let us define $\ddot{X}_d, \dot{X}_d$ and X_d as the desired acceleration, velocity and position of the thumb-tip respectively. Then, we can write PD control law as

$$\ddot{X} = \ddot{X}_d + K_p e + K_v \dot{e} \tag{35}$$

, where $\ddot{X}$ is the actual acceleration of the thumb-tip and $e = X_d - X$ is the error between the position of the thumb tip and the desired thumb position along the trajectory. K_p and K_v are the proportional and the derivative gains respectively.

From equation (33), we have

$$\dot{X} = J\dot{\theta}_a \tag{36}$$

Differentiating, we get

$$\ddot{X} = \dot{J}\dot{\theta}_a + J\ddot{\theta}_a \tag{37}$$

Thus, from equations (35) and (37), we have

$$J\ddot{\theta}_a + \dot{J}\dot{\theta}_a = \ddot{X}_d + K_p e + K_v \dot{e} \tag{38}$$

$$\therefore \ddot{\theta}_a = J^{\dagger}[(\ddot{X}_d - \dot{J}\dot{\theta}_a) + K_p e + K_v \dot{e}] \tag{39}$$

, where $J^{\dagger}$ is the weighted pseudoinverse of J and is a 5×3 matrix. Essentially, equation (39) is a modified form of the classical proportional-derivative controller and it makes the initial error in the desired trajectory converge to zero, with the choice of appropriate gains. The control flow diagram for the closed loop inverse kinematics algorithm is shown in Figure 19.

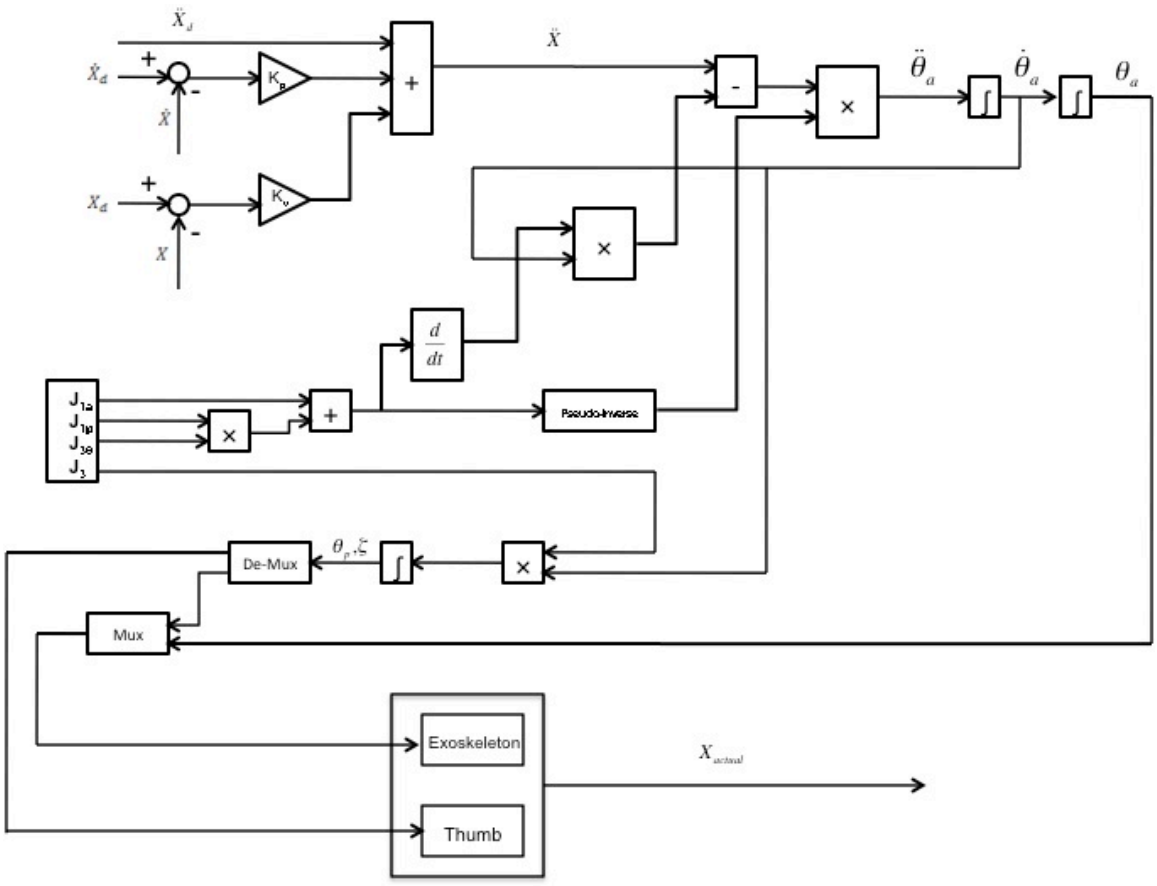

Figure 19 Control flow diagram for CILK

The following plots show the result of the closed-loop inverse kinematics simulation.

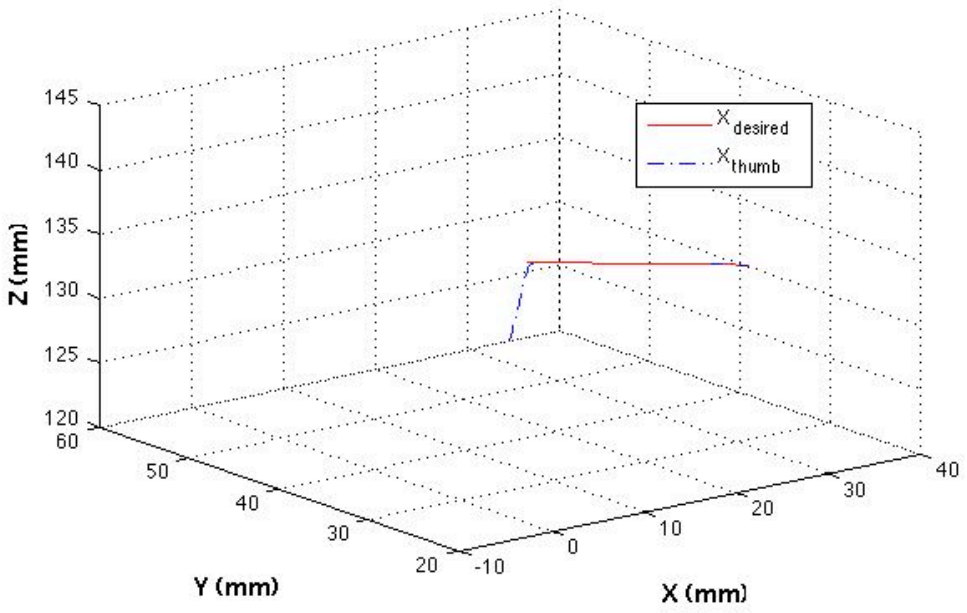

Figure 20 Trajectory of the thumb-tip (CLIK)

In Figure 20, a three-dimensional plot of the thumb-tip trajectory is shown. It can be seen that error in the desired trajectory reduces to zero and then the thumb-tip follows the pre-defined trajectory as expected. To make the above statement more clearer, the following plots show the convergence of the trajectory more clearly.

In figure 21, convergence of errors on individual coordinates (***x***, ***y*** and ***z***) of the trajectories is shown.

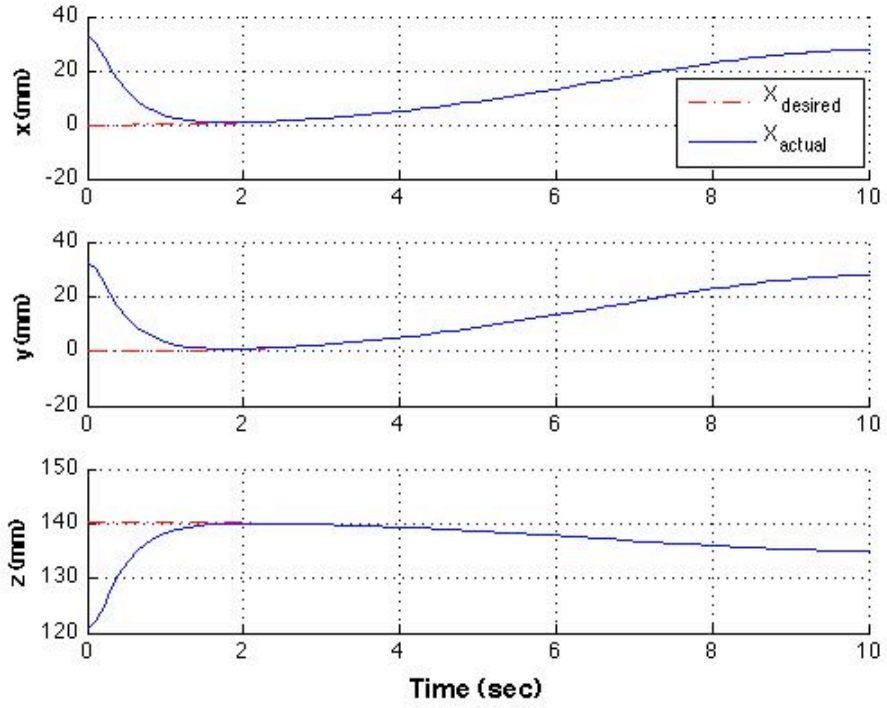

Figure 21 Convergence of the errors in X, Y and Z directions (in mm)

For the Closed-loop inverse kinematics a minimum jerk trajectory is fitted between X_i and X_f and the thumb is initially at the position was at [32.5934; 58.0382; 120.7818] thus introducing an initial error in the trajectory. It can be seen in figure 21 that the initial error in the system converges to zero within the first two sec. The proportional and derivative gains are 20 and 10 respectively.

The constraints on the three bones of the thumb, the metacarpal, proximal phalange and the distal phalange are also satisfied throughout the trajectory. Thus the closed-loop inverse kinematics algorithm works well on the thumb-exoskeleton system.

The error between the thumb and exoskeleton at the three constraints are shown below in Figures 22-24.

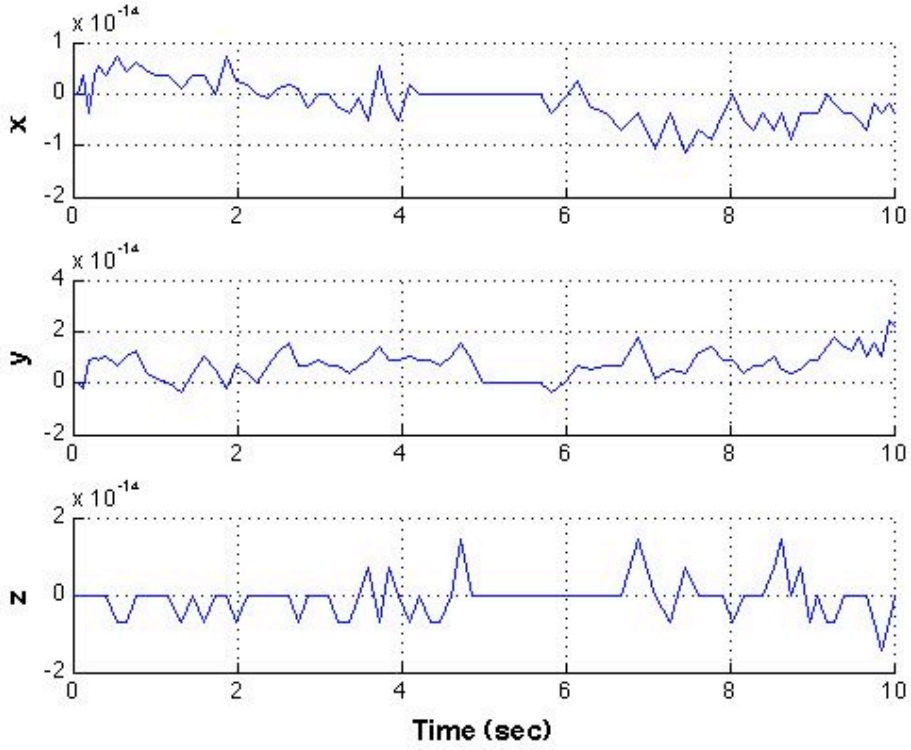

Figure 22 Errors in constraints on metacarpal bone (in mm)

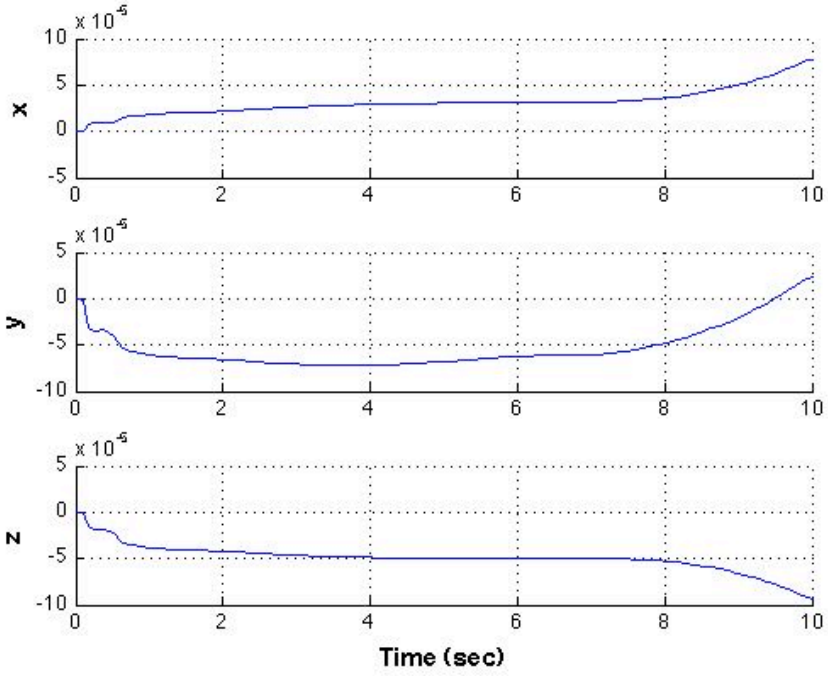

Figure 23 Errors in constraints on proximal phalange (in mm)

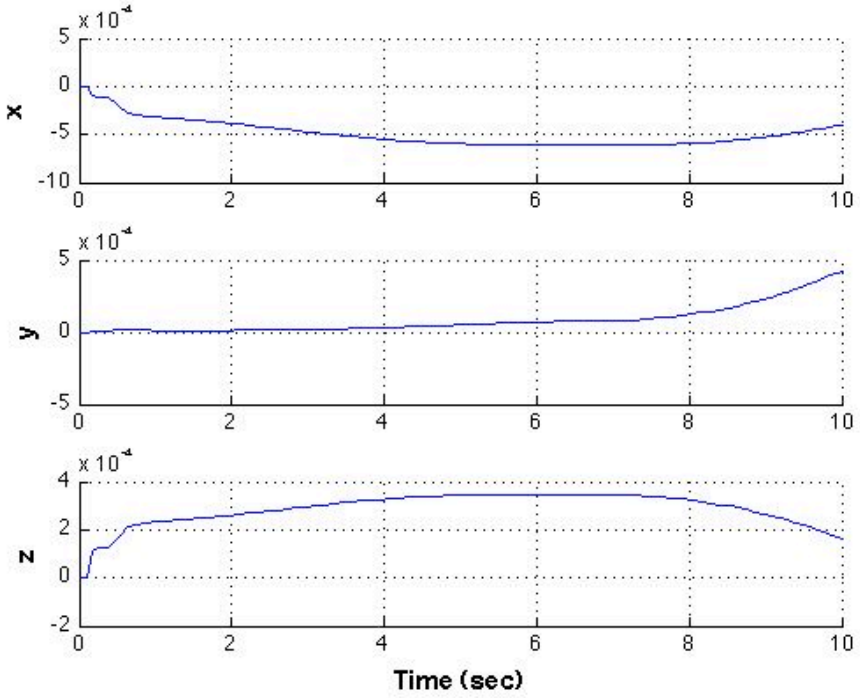

Figure 24 Errors in constraints on distal phalange (in mm)

In the above plots (Figures 22-24) it can be seen that the errors at the constraints are of the order of 10^{-4} mm. These are numerical errors encountered in the calculation, because even if the simulation is carried out for 100 or 150 sec, the errors don't grow unboundedly.

The following plots (Figure 25-27) show the variation of the joint angles of the thumb and the active and passive joint angles of the exoskeleton.

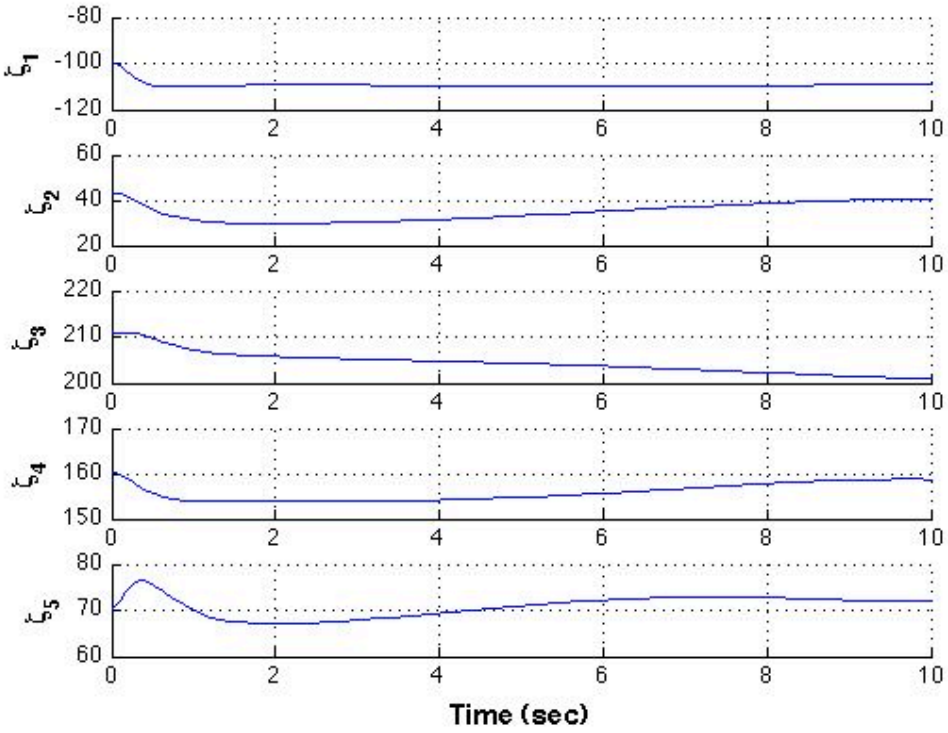

Figure 25 Variation of Joint angles of thumb (in deg) (CLIK)

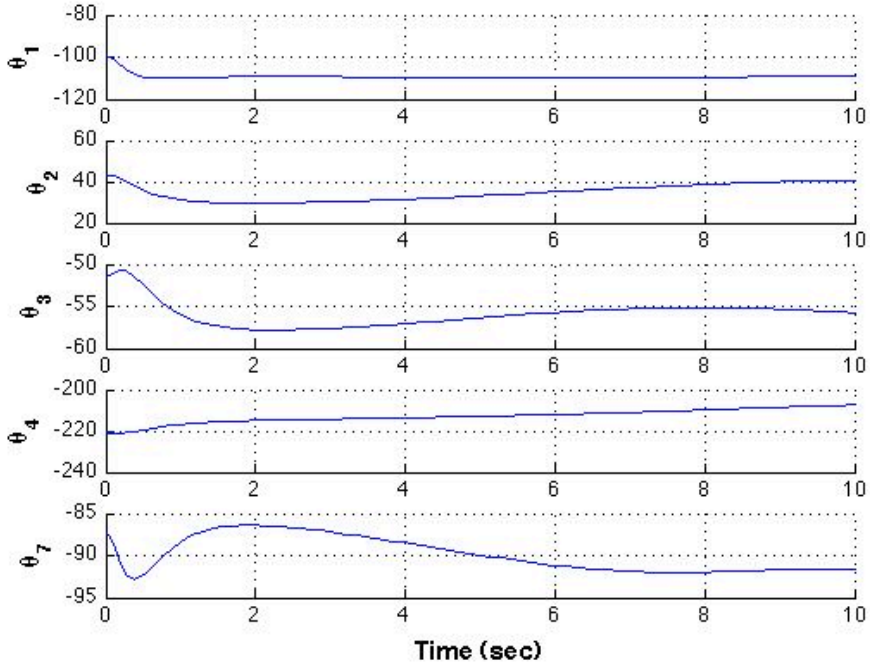

Figure 26 Variation of active angles of exoskeleton (in deg) (CLIK)

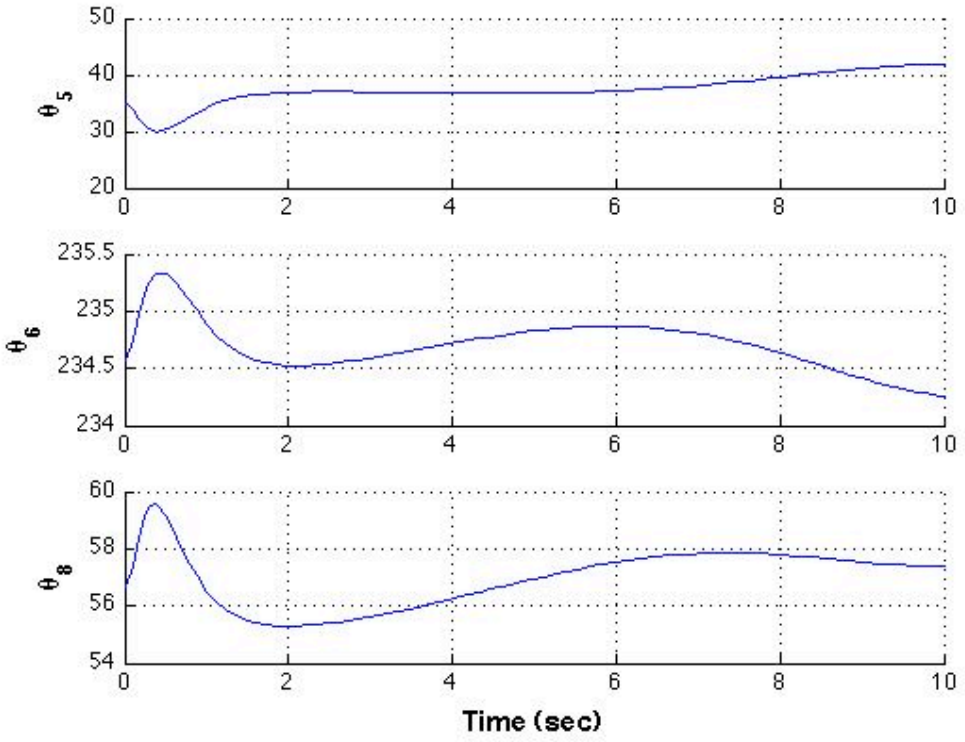

Figure 27 Variation of passive angles of exoskeleton (in deg) (CLIK)

5.2 Joint Limit Avoidance for the redundant manipulator

The thumb is a redundant manipulator with five degrees of freedom and the degree of redundancy of the thumb is two as the end-effector operates in three-dimensional space. Thus,

$$X_3 = G(\zeta_1, \zeta_2, \zeta_3, \zeta_4, \zeta_5) \tag{40}$$

, where X_3 is the end-effector of the thumb and is a 3×1 vector. Differentiating equation (40),

$$\dot{X}_3 = J_{th}\dot{\zeta} \tag{40}$$

, where $J_{th} \in \Re^{3\times5}$ is the Jacobian matrix relating the end-effector velocity with the joint angle velocities of the thumb. The particular solution to equation (40) is obtained by using the pseudoinverse $J_{th}^{\dagger}$ of the matrix J_{th} and the solution can be written as

$$\dot{\xi}_p = J_{th}^{\dagger}\dot{X}_3 \tag{41}$$

where $\dot{\xi}_p$ is the particular solution that is obtained using the pseudoinverse technique. Although, the pseudoinverse technique can offer least-square solution, this particular solution does not guarantee avoidance of singular configurations and joint limits. Another problem with the pseudoinverse solution is that the joint motions generated by this approach do not preserve the repeatability conditions, i.e., a closed path in Cartesian space may not result in a closed path in the joint space. In this problem pertaining to thumb, avoidance of the joint limits of the thumb while performing the natural motion is the major concern. Thus, the redundant degrees of freedom of the thumb are considered along with the null space solutions to setup a systematic procedure for incorporating joint-limit avoidance. The homogeneous solution to the problem $(J_{th}\dot{\xi} = 0)$ in null space can be obtained by the following equation

$$\dot{\xi}_h = (I - J_{th}^{\dagger}J_{th})\dot{\xi}_0 \tag{42}$$

,where the matrix $(I - J_{th}^{\dagger}J_{th})$ is the projector of the joint vector $\dot{\xi}_0$ onto the null-space solution. Thus, by combining the particular (41) and the homogeneous solution (42) the complete inverse solution can be written as

$$\dot{\xi} = \dot{\xi}_p + \dot{\xi}_h \tag{43}$$

The purpose of the inverse solution is to make the end-effector of the thumb follow the desired trajectories in the task space as well as use the redundancy of the thumb to keep

the joints within the joint limits. As mentioned before, the homogeneous solution can be obtained by projecting an arbitrary *n*-dimensional vector (in this case a 5-dimensional vector) ζ_0 to the null space of the Jacobian as in equation (42). In the present literature (Wang and Li, 2009), the typical choice of the null-space joint velocity vector is given by

$$\zeta_0 = \lambda \nabla \Phi(\zeta) = \lambda \frac{\partial \Phi(\zeta)}{\partial \zeta} \tag{44}$$

where $\lambda > 0$ is a scalar, $\Phi(\zeta)$ is a scalar objective function of the joint variables and $\frac{\partial \Phi(\zeta)}{\partial \zeta}$ is the vector function that represents the gradient of $\Phi(\zeta)$. The homogeneous function acts as a gradient optimization method, which converges to a local minimum of the cost function, which can be selected to satisfy the present objective of joint limit avoidance.

For joint limit avoidance let us consider the following cost function (Liegeois, 1977) which models distances from the mechanical joint limits,

$$\Phi(\zeta) = \frac{1}{n} \sum_{i=1}^{n} \left(\frac{\zeta_i - \overline{\zeta}_i}{\zeta_{iM} - \zeta_{im}} \right)^2 \tag{45}$$

where *n*= number of joints (5 in case of thumb), ζ_{iM} and ζ_{im} are the maximum and the minimum joint limits of the i^{th} joint and $\overline{\zeta}_i$ is the middle value of the joint range.

5.3 Redundancy Resolution at Velocity and Acceleration Levels

For a kinematically redundant manipulator, redundancy resolution at velocity level has been studied in depth by many researchers. The joint velocity vector is given by

$$\dot{\zeta} = J_{th}^{\dagger}(\dot{x}_d + K_p(x_d - x)) + (I - J_{th}^{\dagger} J_{th})\dot{\zeta}_0 \tag{46}$$

where $x_d \in \Re^{3\times1}$ is the desired trajectory of the end-effector in the Cartesian space, K_p is the proportional constant of the generic proportion controller and α_0 is given by equation (44).

In the present research, we have extended the Closed Loop Inverse Kinematics (CLIK) algorithm to incorporate joint limits in the manipulator. But if the redundancy resolution is accomplished only at the velocity level, PD- controller cannot be used to achieve the desired task. So, the redundancy resolution scheme should be extended to the acceleration level. The general solution for joint acceleration is given by

$$\ddot{\xi} = J_{th}^{\dagger}(\ddot{X} - \dot{J}_{th}\dot{\xi}) + (I - J_{th}^{\dagger}J_{th})\varphi \tag{47}$$

where $\ddot{X} = \ddot{X}_d + K_v(\dot{X}_d - \dot{X}) + K_p(X_d - X)$ and $\varphi \in \Re^{5\times1}$ is an arbitrary vector in the joint space of the thumb. It should be noted that the basic difference between equation (46) and (47) is the differential order at which redundancy resolution is achieved.

Unlike velocity-level redundancy resolution, while considering redundancy at acceleration level, it is mandatory to consider the objective function of the form $\Phi(\xi, \dot{\xi})$, which depend both on joint velocity and configuration. It can be observed that the general acceleration solution, that is, the equation (47) is the exact constrained minimizer of the following quadratic function (Luca, Oriolo & Siciliano, 1992)

$$L(\xi, \dot{\xi}, \ddot{\xi}) = \frac{1}{2}\ddot{\xi}^T\ddot{\xi} - \varphi^T(\xi, \dot{\xi})\ddot{\xi} \tag{48}$$

A reasonable choice of φ in equation (48) is the one, which contains separate contribution of joint velocity and the configuration of the thumb. Thus, we choose a mixed objective function as

$$\Phi'(\zeta,\dot{\zeta}) = \frac{1}{2}\dot{\zeta}^T K_v \dot{\zeta} + \Phi(\zeta) \tag{49}$$

and "blending" the negative gradients into φ as

$$\begin{aligned} \varphi &= -\nabla_\zeta \Phi' - \lambda \nabla_\zeta \Phi' \\ &= -K\dot{\zeta} - \lambda \nabla_\zeta \Phi \end{aligned} \tag{50}$$

The structure of equation (50) is motivated by the desire to damp the joint velocities (with K>0) in the Jacobian null-space, while trying to optimize the configuration dependent criterion Φ. The scaling factor λ establishes the relative importance between the two objectives. Thus, the final acceleration solution can be written as

$$\ddot{\zeta} = J_{th}^{\dagger}(\ddot{X}_d + K_v(\dot{X}_d - X) + K_p(X_d - X) - \dot{J}_{th}\dot{\zeta}) - (I - J_{th}^{\dagger}J_{th})(K\dot{\zeta} + \lambda \nabla_\zeta \Phi) \tag{51}$$

where Φ is defined in the same way as in equation (45) and its purpose is to keep the thumb configuration within the joint limits. Researchers (Luca, Oriolo & Siciliano, 1992) used the equations 48-50 to solve kinematic redundancy at acceleration level to achieve enhanced task trajectory tracking performance. In our case, we have used these equations coupled with equation 45 to satisfy the required joint-limit avoidance for the thumb.

Integrating equation (51) gives the joint angle velocities of the thumb $\dot{\zeta}$. Also, the joint angle velocities of the thumb and the exoskeleton are related by equations (30) and (31). The active joint angle velocities of the exoskeleton from equation (30) is given by

$$\dot{\theta}_a = J_{\theta_a}^{-1}\dot{\zeta} \tag{52}$$

where $J_{\theta a} \in \Re^{5\times5}$ is the Jacobian matrix. Once the active joint angle velocities are computed, equation (31) gives the passive joint angle velocities of exoskeleton. The angular velocities when integrated with a feasible initial condition generate the

appropriate thumb-exoskeleton motion on the desired trajectory in the Cartesian space. The control flow diagram is shown in the Figure 28.

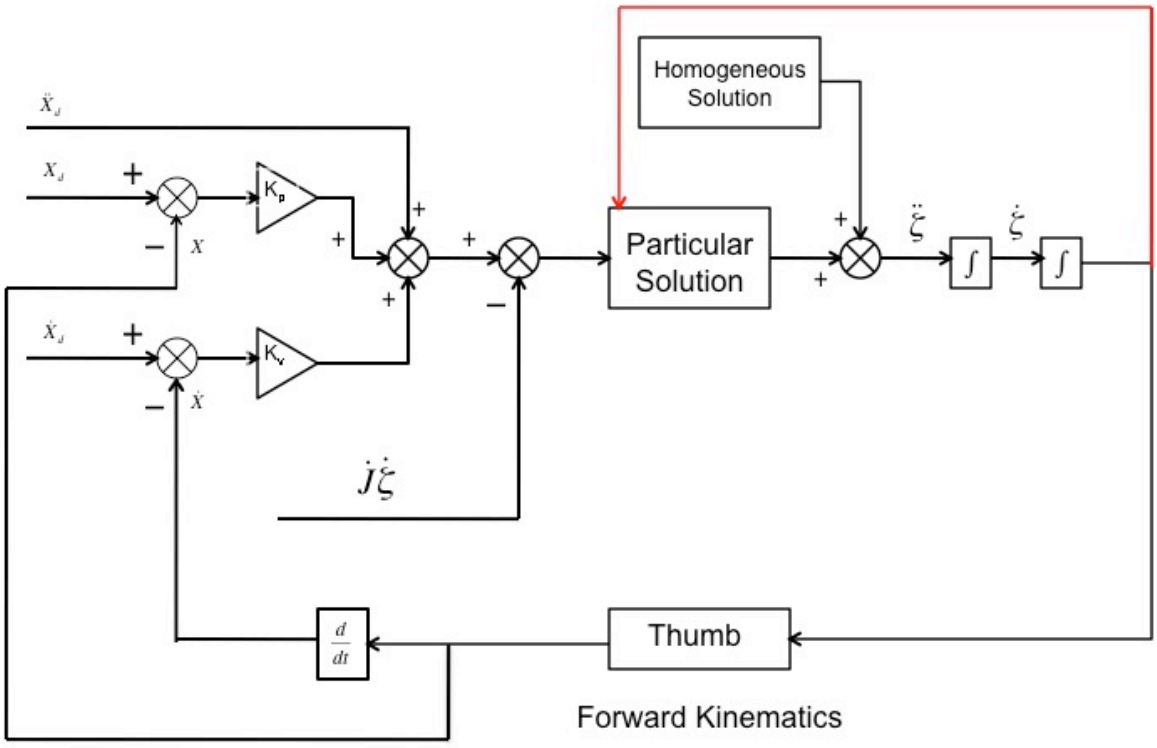

Figure 28 Redundancy Resolution

5.4 Results

The results of kinematic redundancy resolution for joint-limit avoidance is shown and discussed in the following plots. The thumb tip (exoskeleton tip) is made to follow a trajectory between the points $\boldsymbol{X_i}$=[-0.0293; 22.4897; 140.2753] and $\boldsymbol{X_f}$=[27.6707; -26.3365; 135.0360]. The thumb-tip is initially at $\boldsymbol{X_s}$=[32.5934; 58.0382; 135.0360] introducing an initial error in the desired trajectory.

The following plots (figure 29 and 30) show the path tracked by the thumb-tip and the convergence of error, when closed loop inverse kinematics with redundancy resolution is applied at acceleration level. The proportional and the derivative gains were 20 and 10 respectively. Also the scalar constants $\boldsymbol{K}$ and λ were 20 and 100. It can be seen that the errors in the desired and the actual trajectory converges to zero during the motion.

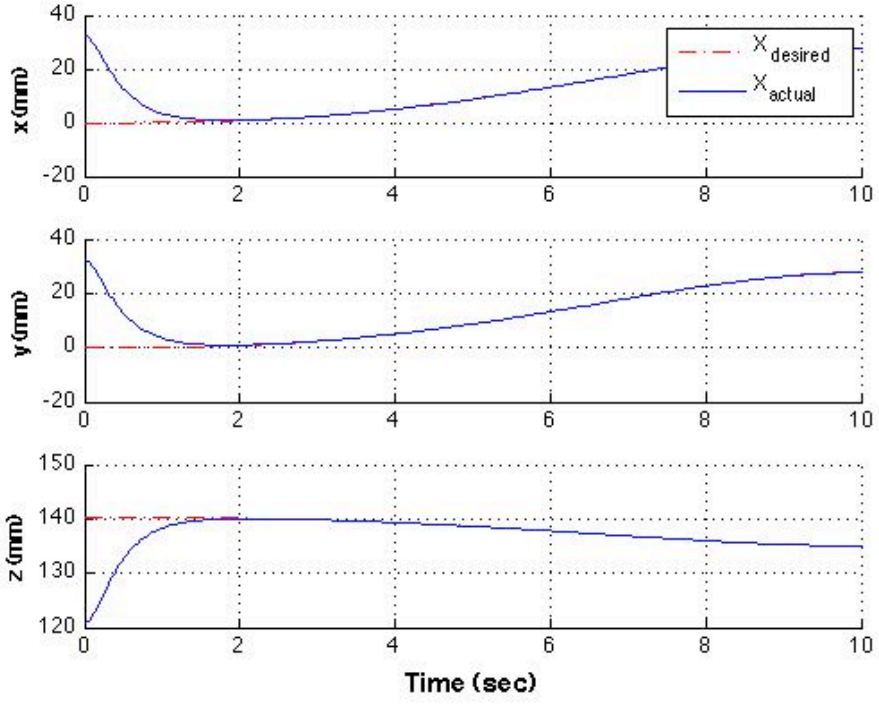

Figure 29 Trajectory of the thumb tip in Cartesian Space (in mm)

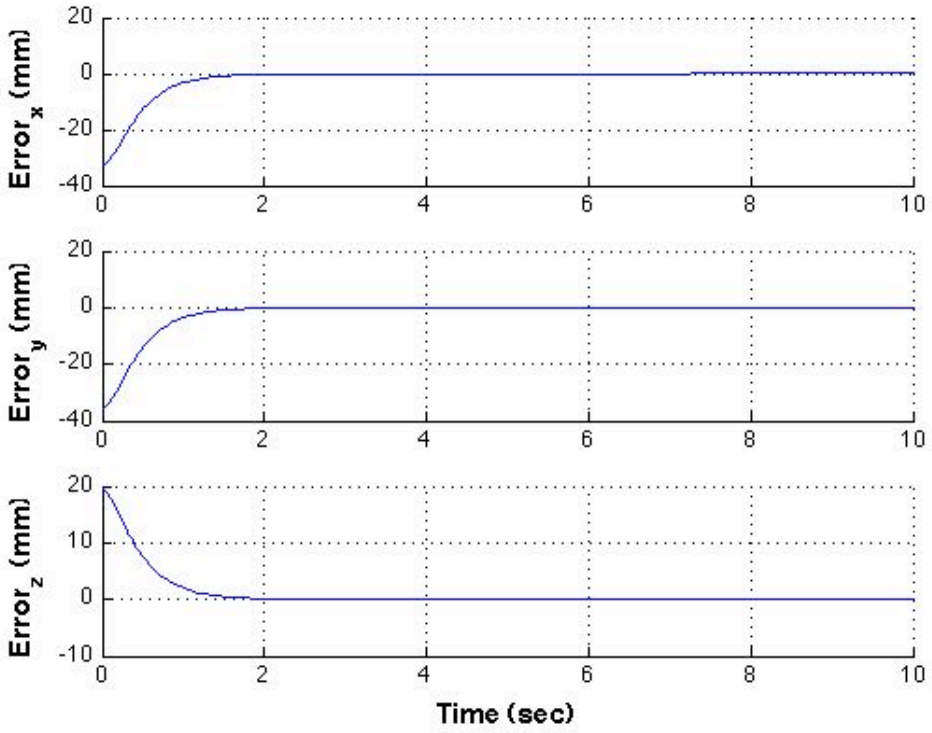

Figure 30 Convergence of Errors in the desired and actual trajectory (in mm)

The error between the thumb and the exoskeleton are shown in the Figures 31-33. At all the three constraints the errors were found to be of the order of 10^{-5} mm.

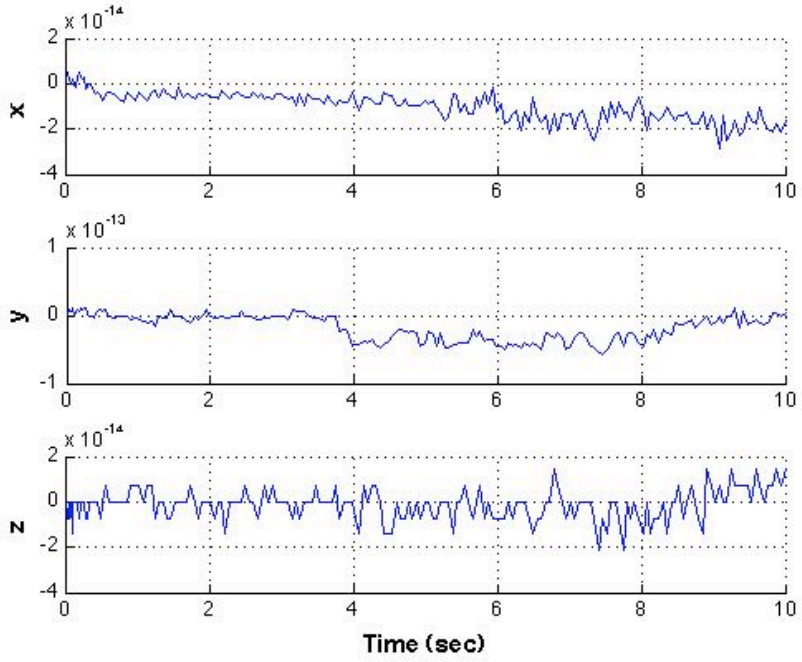

Figure 31 Errors in constraint on metacarpal bone

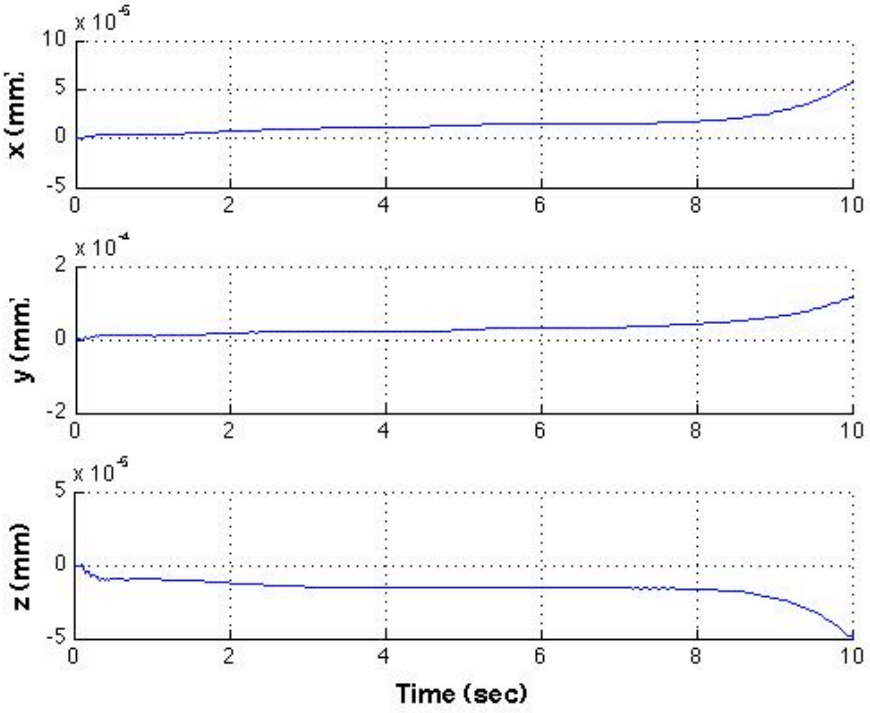

Figure 32 Errors in constraint on distal phalange

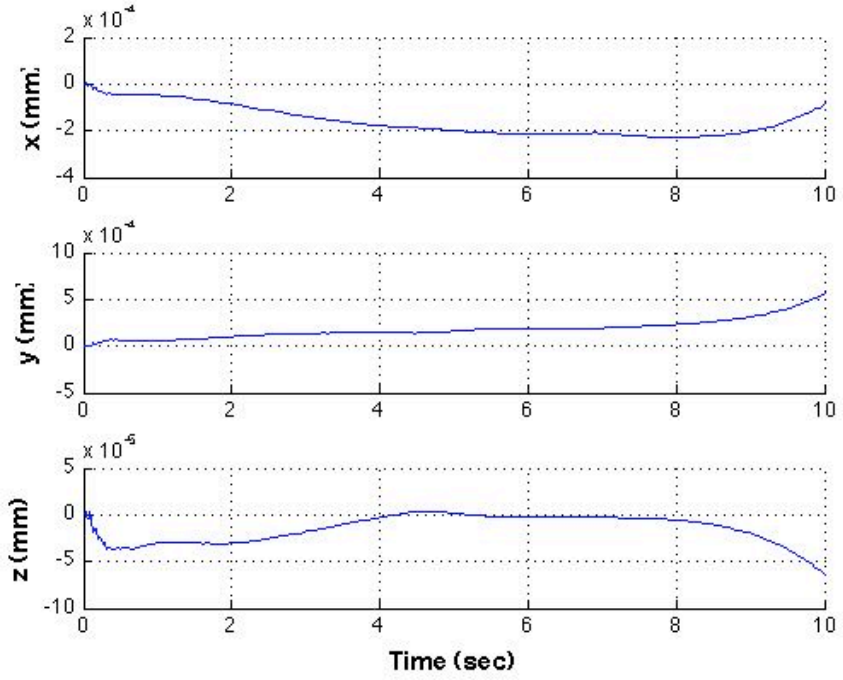

Figure 33 Errors in constraint on distal phalange

The following plot (figure 34) shows the variations in the thumb joint angles. The joint limits on the thumb, are tabulated below

Table 4 Range of motion of thumb

Joint	Lower limit (deg)	Higher limit (deg)	Effective range (deg)	Reference Value (deg)
CMC FE axis (ζ_1)	-119.22	-174.22	55	-104.22
CMC AA axis (ζ_2)	13.07	53.07	40	21.07
MP FE axis (ζ_3)	200.07	230.07	30	200.07
MP AA axis (ζ_4)	160.35	165.35	5	160.35
IP FE axis (ζ_5)	60.2	150.2	90	70.2

The zero position of the thumb refers to the straight thumb configuration as shown in Figure 5. The upper and the lower limits on the joint angles are found by distributing the range across the reference position of the Type II thumb (Santos & Valero-Cuevas,

2006). It should be noted in Figure 34 that the joint angles of the thumb are within the range of motion of thumb as expected, because of redundancy resolution at acceleration level. In figure 35 and 36 the corresponding active and passive joint angles of the exoskeleton are shown.

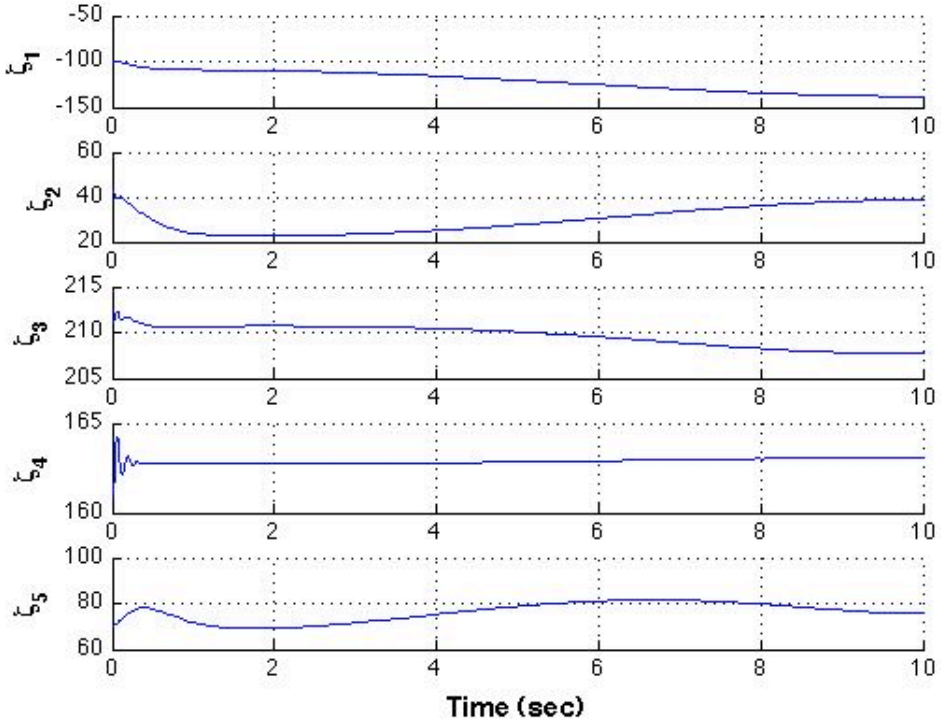

Figure 34 Variation of joint angles of thumb (in deg)

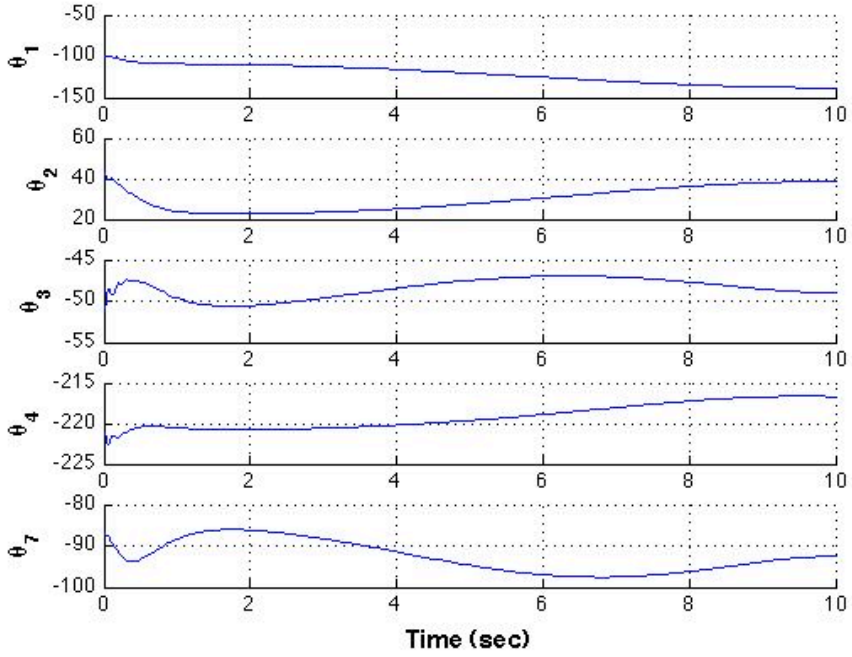

Figure 35 Variation of active joint angles of the exoskeleton (in deg)

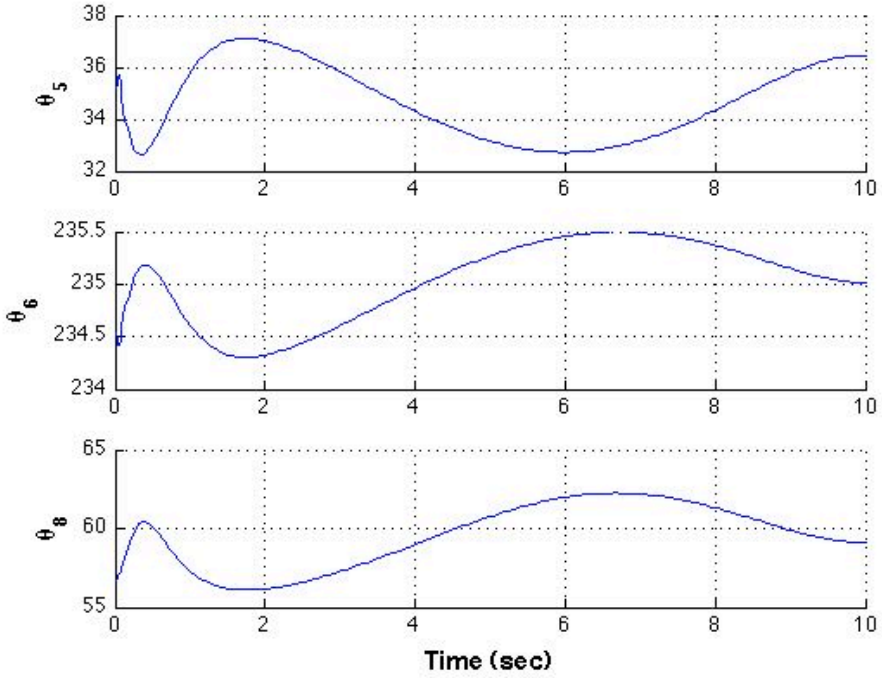

Figure 36 Variation of passive angles of the exoskeleton (in deg)

5.5 Comparison of Motion of thumb with and without the application of Joint Limits

At the end, a comparison of both the closed loop inverse kinematics algorithm with and without the application of redundancy resolution techniques for the same trajectory in the Cartesian space is presented. As mentioned previously a minimum jerk trajectory is fitted between the points X_i=[-0.0293; 22.4897; 140.2753] and X_f =[27.6707; -26.3365; 135.0360]. It can be seen clearly that for the latter the joint angles of the thumb remain within the defined limits while following the trajectory.

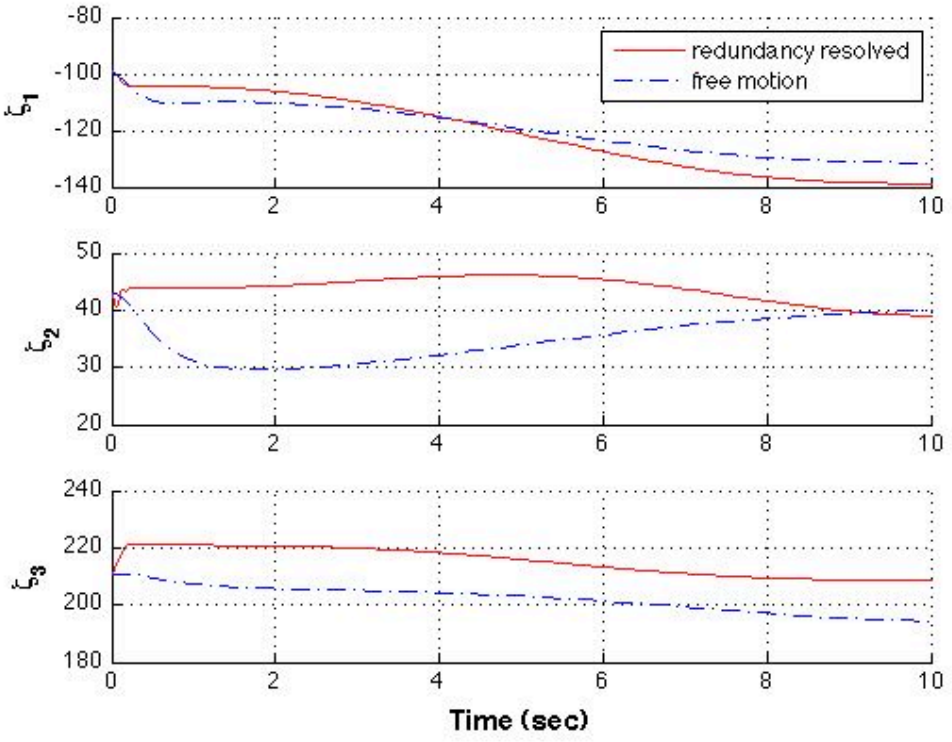

Figure 37 Comparison of joint angles of thumb (in deg) (1 of 2)

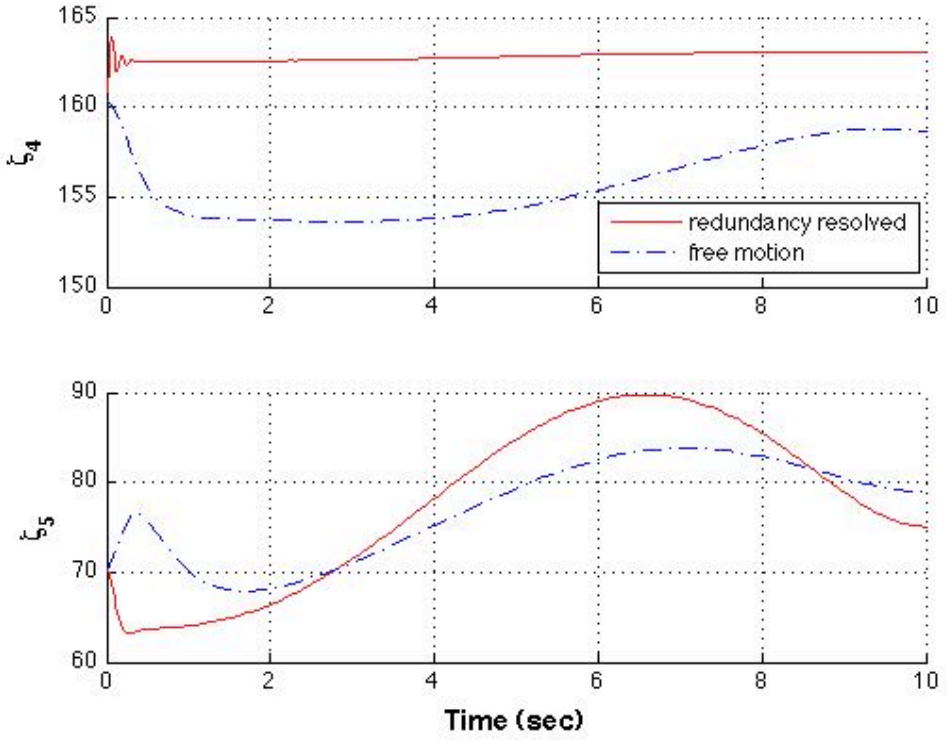

Figure 38 Comparison of joint angles of thumb (in deg) (2 of 2)

It can be seen in figure 37 that the MP FE (metacarpophalangeal flexion/extension (ζ_3)) joint goes off limits towards the end of trajectory. The lower limit for MP FE joint is 200.7 degree. Also huge off-limit motion of the MP AA (metacarpophalangeal adduction/abduction (ζ_4)) joint is observed through out the trajectory. But, when redundancy resolution is applied all the three joint angles remain with the joint limits specified in table 4. It should be noted that the thumb-tip follows the pre-defined trajectory closely in both the cases as desired irrespective of application of redundancy resolution.

CHAPTER VI

CONTRIBUTIONS AND FUTURE WORK

In this thesis, a general framework for mathematical modeling of thumb and exoskeleton for rehabilitation is discussed. The thumb model is based on the Denavit-Hartenberg (DH) parameters found in a recent study (Santos & Valero-Cuevas, 2006). The thesis validates the exoskeleton designed for rehabilitation of the thumb through simulation and applies a kinematic control scheme for the exoskeleton, which in effect controls the individual joints of the thumb independently. The present model of thumb takes into account all the five DOFs of thumb, unlike previous models which only considered three or four degrees of freedom ruling out the adduction/abduction motions at the CMC and/or the MCP joints.

6.1 Contributions

An exoskeleton has been designed for the thumb, which takes into account the anatomical variability of the thumb throughout the population. In this thesis, a kinematic analysis of the coupled motion of the thumb-exoskeleton system is discussed. The kinematic redundancy of the thumb-exoskeleton system is exploited to address the secondary task of retaining the thumb motion within the joint limits of natural motion, while executing the primary task of following a desired trajectory. A Closed-loop Inverse Kinematics algorithm has been implemented successfully for the kinematic control of the thumb

motion. But, this approach had a problem of thumb joints off-shooting the normal limits of joint motion of thumb.

With thumb being a redundant manipulator with a degree of redundancy two, the above problem was overcome by utilizing the null space solution of the inverse kinematics. Previous studies show redundancy resolution schemes at velocity level to limit the motion of a redundant manipulator within the joint limits, but the redundancy resolution scheme for joint limit avoidance was extended to the acceleration level in this thesis and successfully implemented.

6.2 Future Work

The motion of the thumb is complex and it is very difficult to determine the inertia properties of the different segments of the thumb. A dynamic control scheme for the control of thumb needs to be formulated. These control schemes should also be adaptive in order to take into account the variability of uncertain inertia properties of the thumb,

In this thesis, the issue of pose control of the thumb remains unaddressed. In our control scheme, only the position of the thumb-tip is controlled. But, if the pose control is also taken into account, the thumb no longer remains a redundant system, but offers a unique solution. Also, the effect of muscle interaction between the thumb and exoskeleton needs to be answered. On a broader scale, it remains to be seen how to use this device for rehabilitation on patients. Should this device assist in motion or resist motion. The effects of error augmentation techniques on thumb rehabilitation should also be investigated. The device needs to be tested on actual patients for coordinated control of the different joints of the thumb.

REFERENCES

Azadeh, K., Andrew, M., Christina, T., Brian, W., Loukas, A., Tzika, A., et al. (2006). fMRI-compatible rehabilitation hand device. *Journal of NeuroEngineering and Rehabilitation* .

Baillieul, J., Hollerbach, J., & Brockett, R. (1984, Jan 1). Programming and control of kinematically redundant manipulators. *Decision and Control* .

Baker, D., & Wampler, C. (1988, Jan 1). On the inverse kinematics of redundant manipulators. *The International Journal of Robotics Research* .

Brown, P., Jones, D., Singh, S., & Rosen, J. (1993, Jan 1). The exoskeleton glove for control of paralyzed hands. *1993 IEEE International Conference on Robotics and Automation* .

Cooney, W., & Chao, E. (1977, Jan 1). Biomechanical analysis of static forces in the thumb during hand function. *The Journal of Bone And Joint Surgery* .

Esteki, A., & Mansour, J. (1997, Jan 1). A dynamic model of the hand with application in functional neuromuscular Stimulation. *Annals of biomedical engineering* .

Foreman, N., Wilson, P., & Stanton, D. (1997, Jan 1). VR and spatial awareness in disabled children. *Communications of the ACM* .

Giurintano, D., Hollister, A., & Buford, W. (1995, Jan 1). A virtual five-link model of the thumb. *Medical Engineering and Physics* .

Holden, M., Dyar, T., Schwamm, L., & Bizzi, E. (2003, Jan 1). Home-based telerehabilitation using a virtual environment system. *... workshop on virtual ...* .

Hollister, A., Buford, W., & Myers, L. (2005, Jan 1). The axes of rotation of the thumb carpometacarpal joint. *Journal of Orthopaedic Research* .

Hsu, P., Hauser, J., & Sastry, S. (1988, Jan 1). Dynamic control of redundant manipulators. *1988 IEEE International Conference on Robotics and ...* .

Hume, M., Gellman, H., & McKellop, H. (1990, Jan 1). Functional range of motion of the joints of the hand. *The Journal of hand ...* .

Ito, S., Ishigure, Y., Ueki, S., Mizumoto, J., & Nishimoto, Y. (2009, Jan 1). A hand rehabilitation support system with improvements based on clinical practices. *robo.mech.gifu-u.ac.jp* .

Jack, D., Boian, R., Merians, A., & Adamovich, S. (2000, Jan 1). A virtual reality-based exercise program for stroke rehabilitation. *Proceedings of the the fourth international ACM conference on Assistive technologies* .

Kawasaki, H., Ito, S., & Ishigure, Y. (2007, Jan 1). Development of a Hand Motion Assist Robot for Rehabilitation Therapy by Patient Self-Motion Control. *International Conference on Rehabilitation Robotics* .

Klein, C., & Huang, C. (1983, Jan 1). Review of pseudoinverse control for use with kinematically redundant manipulators. *IEEE Transactions on Systems* .

Lemay, M., & Crago, P. (1996, Jan 1). A dynamic model for simulating movements of the elbow, forearm, and wrist. *Journal of Biomechanics* .

Light, C., & Chappell, P. (2000, Jan 1). Development of a lightweight and adaptable multiple-axis hand prosthesis. *Medical Engineering and Physics* .

Luca, A. D., Oriolo, G., & Siciliano, B. (1992). Robot Redundancy Resolution at the Acceleration Level. *Laboratory Robotics and Automation , 4*, 97--97.

Masia, L., Krebs, H., Cappa, P., & Hogan, N. (2007, Jan 1). Design and Characterization of Hand Module for Whole-Arm Rehabilitation Following Stroke. *IEEE/ASME Transactions on Mechatronics* .

O'dell, M., Lin, C.-C., & Harrison, V. (2009). Stroke Rehabilitation: Strategies to Enhance Motor Recovery. *Annual Review of Medicine , 60* (1), 55-68.

Park, D., Lee, S., Kim, S., & Kwak, Y. (2003, Jan 1). Torque distribution using a weighted pseudoinverse in a redundantly actuated mechanism. *Advanced Robotics* .

Paul, R., & Shimano, B. (1978). Kinematic control equations for simple manipulators. *1978 IEEE Conference on Decision and Control including the 17th Symposium on Adaptive Processes , 17*.

Riener, R., Nef, T., & Colombo, G. (2005, Jan 1). Robot-aided neurorehabilitation of the upper extremities. *Medical and Biological Engineering and Computing* .

Sancho-Bru, J., Perez-Gonzalez, A., Vergara-Monedero, M., & Giurintano, D. (2001, Jan 1). A 3-D dynamic model of human finger for studying free movements. *Journal of Biomechanics* .

Santos, V., & Valero-Cuevas, F. (2006, Jan 1). Reported Anatomical Variability Naturally leads to multimodal distributions of Denavit-Hartenberg parameters for the human thumb. *IEEE Transactions on Biomedical Engineering* .

Shuang, W., Jiting, L., Yuru, Z., & Ju, W. (n.d.). Active and Passive Control of an Exoskeleton with Cable Transmission for Hand Rehabilitation. *haptic.buaa.edu.cn* .

Siciliano, B. (1990, Jan 1). Kinematic control of redundant robot manipulators: A tutorial. *Journal of Intelligent and Robotic Systems* .

Taylor, R. (1979, Jan 1). Planning and execution of straight line manipulator trajectories. *IBM Journal of Research and Development* .

Wang, J., & Li, Y. (n.d.). Comparative Analysis for the Inverse Kinematics of Redundant Manipulators based on Repetitive Tracking Tasks.

Yoshikawa, T. (1984, Jan 1). Analysis and control of robot manipulators with redundancy. *Robotics Research: The First International Symposium* .